11

NEUTRON AND NUCLEAR TECHNIQUES

11.0 INTRODUCTION

All the techniques discussed here involve the atomic nucleus. Three use neutrons, generated either in nuclear reactors or very high energy proton accelerators (spallation sources), as the probe beam. They are Neutron Diffraction, Neutron Reflectivity, NR, and Neutron Activation Analysis, NAA. The fourth, Nuclear Reaction Analysis, NRA, uses charged particles from an ion accelerator to produce nuclear reactions. The nature and energy of the resulting products identify the atoms present. Since NRA is performed in RBS apparatus, it could have been included in Chapter 9. We include it here instead because nuclear reactions are involved.

Neutron diffraction uses neutrons of wavelengths 1–2 Å, similar to those used for X-rays in XRD (Chapter 4), to determine atomic structure in crystalline phases in an essentially similar manner. There are several differences that make the techniques somewhat complementary, though the need to go to a neutron source is a significant drawback. Because neutrons are diffracted by the nucleus, whereas X-ray diffraction is an electron density effect, the neutron probing depth is about 10^4 longer than X-ray. Thus neutron diffraction is an entirely bulk method, which can be used under ambient pressures, and to analyze the interiors of very large samples, or contained samples by passing the neutron flux through the containment walls. Along with this capability, however, goes the difficulty of neutron shielding and safety. Where X-ray scattering cross sections increase with the electron density of the atom, neutron scattering varies erratically across the periodic table and is

approximately equal for many atoms. As a result, neutron diffraction "sees" light elements, such as oxygen atoms in oxide superconductors, much more effectively than X-ray diffraction. A further difference is that the neutron magnetic moment strongly interacts with the magnetic moment of the sample atoms, allowing determination of the spatial arrangements of magnetic moments in magnetic material. The equivalent interaction with X rays is a factor of 10^6 weaker. Neutron diffraction has proved useful in studying thin magnetic multilayers because, though it is a bulk technique, the magnetic scattering interactions are strong enough to enable usable data to be taken for as little as 500-Å thicknesses for metals.

In Neutron Reflectivity the neutron beam strikes the sample at grazing incidence. Below the critical angle (around 0.1°), total reflection occurs. Above it, reflection in the specular direction decreases rapidly with increasing angle in a manner depending on the neutron scattering cross sections of the elements present and their concentrations. On reaching a lower interface the transmitted part of the beam will undergo a similar process. H and D have one of the largest "mass contrasts" in neutron-scattering cross section. Thus, if there is an interface between a H-containing and a D-containing hydrocarbon, the reflection-versus-angle curve will depend strongly on the interface sharpness. Thus interdiffusion across hydrocarbon material interfaces can be studied by D labeling. For polymer interfaces the depth resolution obtained this way can be as good as 10 Å at buried interface depths of 100 nm, whereas the alternative techniques available for distinguishing D from H at interfaces, SIMS (Chapter 10) and ERS (Chapter 9), have much worse resolution. Also, neutron reflection is performed under ambient pressures, whereas SIMS and ERS require vacuum conditions. Labeling is not necessary if there is sufficient neutron "mass contract" already available—e.g., interfaces between fluorinated hydrocarbons and hydrocarbons. The technique has also been used for biological films and, magnetic thin films, using polarized neutron beam sources, where the magnetic gradient at an interface can be determined.

Though a powerful technique, Neutron Reflectivity has a number of drawbacks. Two are experimental: the necessity to go to a neutron source and, because of the extreme grazing angles, a requirement that the sample be optically flat over at least a 5-cm diameter. Two drawbacks are concerned with data interpretation: the reflectivity-versus-angle data does not directly give a a depth profile; this must be obtained by calculation for an assumed model where layer thickness and interface width are parameters (cf., XRF and VASE determination of film thicknesses, Chapters 6 and 7). The second problem is that roughness at an interface produces the same effect on specular reflection as true interdiffusion.

In NAA the sample is made radioactive by subjecting it to a high dose (days) of thermal neutrons in a reactor. The process is effective for about two-thirds of the elements in the periodic table. The sample is then removed in a lead-shielded container. The radioisotopes formed decay by B emission, γ-ray emission, or X-ray emission. The γ-ray or X-ray energies are measured by EDS (see Chapter 3) in spe-

cial laboratories equipped to handle radioactive materials. The energies identify the elements present. Concentrations are determined from peak intensities, plus knowledge of neutron capture probabilities, irradiation dose, time from dose, and decay rates. The technique is entirely bulk and is most suitable for the simultaneous detection of trace amounts of heavy elements in non-γ-ray emitting hosts. Since decay lifetimes can be very variable it is sometimes possible to greatly improve detection limits by waiting for a host signal to decay before measuring that of the trace element. This is true for Au in Si where levels of 3×10^7 atoms/cc are achieved. An As- or Sb-doped Si, host would give much poorer limits for Au, however, because of interfering signals from the dopants.

In NRA a beam of charged particles (e.g., H, N, or F) from an ion accelerator at energies between a few hundred keV and several MeV (cf., RBS, Chapter 9) induces nuclear reactions for specific light elements (up to Ca). Various particles (protons, α particles, etc.) plus γ-rays are released by the process. The particles are detected as in RBS and, similarly their yield-versus-energy distribution identifies the element and its depth distribution. This can provide a rapid nondestructive, analysis for these elements, including H. The depth probed can be up to several μm with a re- solution varying from a few tens of nanometers at the surface to hundreds of nanometers at greater depths. Usually there is no lateral resolution, but a microbeam systems with a few-micron capability exist. If particle detection is too inefficient (too low energies), γ-ray spectroscopy (cf., NAA) can yield elemental concentration, but not depth distributions. For some elements the nuclear reaction process has a maximum in its cross section at a specific beam energy, E_R (resonance energy). This provides an alternative method of depth profiling (resonance profiling), since if the incident beam energy, E_0, is above E_R, it will drop to E_R at a specific reaction distance below the surface (electronic energy losses, see RBS). By changing E_0 the depth at which E_R is achieved is changed, and so the depth at which the analyzed particles are produced is changed. Resonance profiling can have better sensitivity than nonresonance, but the depth resolution depends on the energy width of the resonance.

11.1 Neutron Diffraction

RAYMOND G. TELLER

Contents

Introduction

Since the recognition in 1936 of the wave nature of neutrons and the subsequent demonstration of the diffraction of neutrons by a crystalline material, the development of neutron diffraction as a useful analytical tool has been inevitable. The initial growth period of this field was slow due to the unavailability of neutron sources (nuclear reactors) and the low neutron flux available at existing reactors. Within the last decade, however, increases in the number and type of neutron sources, increased flux, and improved detection schemes have placed this technique firmly in the mainstream of materials analysis.

As with other diffraction techniques (X-ray and electron), neutron diffraction is a nondestructive technique that can be used to determine the positions of atoms in crystalline materials. Other uses are phase identification and quantitation, residual stress measurements, and average particle-size estimations for crystalline materials. Since neutrons possess a magnetic moment, neutron diffraction is sensitive to the ordering of magnetically active atoms. It differs from many site-specific analyses, such as nuclear magnetic resonance, vibrational, and X-ray absorption spectroscopies, in that neutron diffraction provides detailed structural information averaged over thousands of Å. It will be seen that the major differences between neutron diffraction and other diffraction techniques, namely the extraordinarily

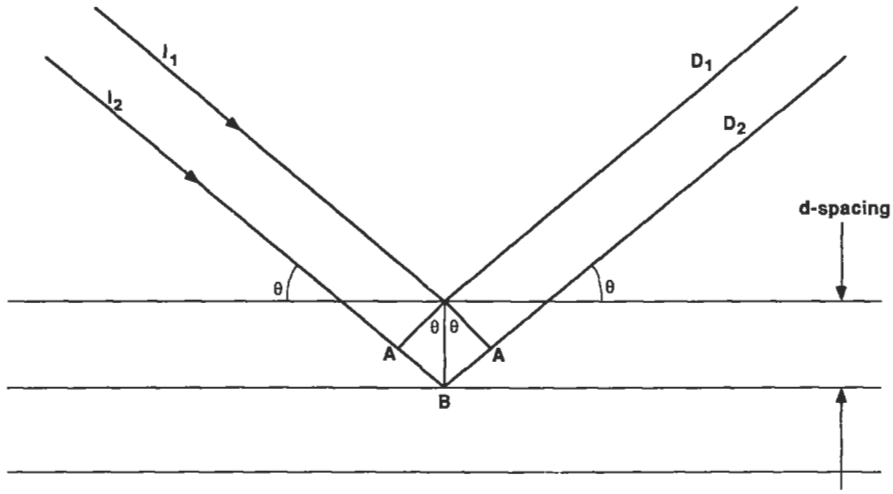

Figure 1 **Bragg diffraction. A reflected neutron wavefront (D_1, D_2) making an angle θ with planes of atoms will show constructive interference (a Bragg peak maxima) when the difference in path length between D_1 and D_2 ($2\overline{AB}$) equals an integral number of wavelengths λ. From the construction, $\overline{AB} = d \sin \theta$.**

greater penetrating nature of the neutron and its direct interaction with nuclei, naturally lead to its superior usage in experiments on materials requiring a penetration depth greater than about 50 μm. Neutron diffraction is especially well suited for structural analysis of materials containing atoms of widely varying atomic number, such as heavy metal oxides.

Basic Principles

Like X-ray and electron diffraction, neutron diffraction is a technique used primarily to characterize crystalline materials (defined here as materials possessing long-range order). The basic equation describing a diffraction experiment is the Bragg equation:

$$\lambda = 2d\sin\theta \tag{1}$$

where d represents the spacing between planes of atoms in the material in the neutron beam, λ is the wavelength of the impinging neutron wavefront, and 2θ is the diffracting angle. The diffraction geometry is illustrated in Figure 1. Inspection of the figure demonstrates that a diffraction maxima (a Bragg peak) is observed when there is constructive interference of the reflected neutron wavefront. The intensities of the Bragg peaks depend strongly upon the nature and number of atoms found lying in the planes responsible for the maxima. Consequently, a diffraction pattern can be obtained by fixing the wavelength of the neutron wavefront and scanning

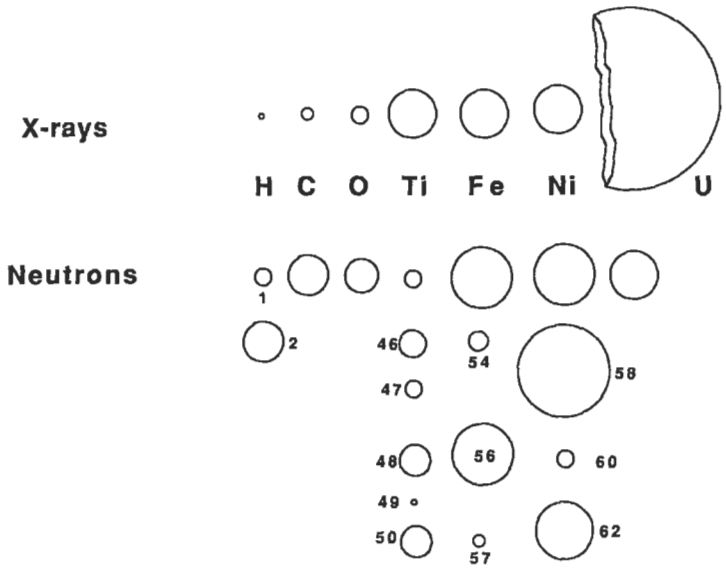

Figure 2 **Scattering physics of X rays and neutrons.**

the angle θ, or alternatively, by fixing θ and scanning a range of neutron wavelengths. It will be seen that both of these modes of operation are used at modern neutron sources.

It should be obvious from Figure 1 that if one wishes to probe *d*-spacings on the order of atomic spacings (Å) that wavelengths of the same length scale are required. Fortunately, X rays, electrons and "thermal" neutrons share the feature of possessing wavelengths of the appropriate size.

An important difference between neutron and X-ray diffraction is the way in which neutrons and X rays interact with matter. X rays are scattered primarily by electrons. Consequently, an X-ray diffraction pattern reflects the distribution of the electron density within a solid. Conversely, neutrons are scattered by nuclei, and the resultant diffraction pattern reflects nuclear distributions. Since the physics of the scattering differs significantly so does the sensitivity of each technique to various elements. While X-ray scattering from an element is roughly proportional to the local electron density (and the atomic number of the target atoms), neutron scattering is nucleus-dependent and can vary erratically as one proceeds through the periodic table. For this reason, X-ray diffraction analysis of heavy metal oxides (such as Bi_2O_3) provides information primarily about the metal atoms, whereas neutron diffraction analysis yields detailed positional information for all elements approximately equally.

One further important difference between neutron and X-ray diffraction is the former's sensitivity to magnetic structure. The magnetic moments of neutrons

interact with the magnetic moments of target atoms, whereas this interaction is much weaker ($\sim 10^{-6}$) for X rays. The interaction strength is proportional to the magnetic moments of the atoms in the material, and depends on their orientation relative to the neutron moment. These features make neutron diffraction the best technique for probing the spatial arrangement of magnetic moments in magnetic materials.

Experimental Considerations

Another major difference between the use of X rays and neutrons used as solid state probes is the difference in their penetration depths. This is illustrated by the thickness of materials required to reduce the intensity of a beam by 50%. For an aluminum absorber and wavelengths of about 1.5 Å (a common laboratory X-ray wavelength), the figures are 0.02 mm for X rays and 55 mm for neutrons. An obvious consequence of the difference in absorbance is the depth of analysis of bulk materials. X-ray diffraction analysis of materials thicker than 20–50 μm will yield results that are severely surface weighted unless special conditions are employed, whereas internal characteristics of physically large pieces are routinely probed with neutrons. The greater penetration of neutrons also allows one to use thick ancillary devices, such as furnaces or pressure cells, without seriously affecting the quality of diffraction data. Thick-walled devices will absorb most of the X-ray flux, while neutron fluxes hardly will be affected. For this reason, neutron diffraction is better suited than X-ray diffraction for *in-situ* studies.

A less obvious consequence of the difference in absorbance between X rays and neutrons is the large difference in the sizes of facilities using the two types of radiation (primarily for reasons of safety). While only a few millimeters of metal are required to assure the safety of workers near an X-ray source, several meters of absorbing material (usually steel, concrete, or boron-containing materials) are required around neutron sources. Because of the shielding requirement, neutron sources and instruments are orders of magnitude larger than the corresponding X-ray devices. While this leads to much greater expense for neutron sources, it also allows the analysis of larger samples. For example, railroad rails and large-circumference pipes have been analyzed for residual stress at the nuclear reactor at Chalk River, Ontario. This work could not have been done on a standard X-ray diffractometer.

Neutron Sources

Two types of sources are used. Originally developed in the 1940s, nuclear reactors provided the first neutrons for research. While reactors provide a continuous source of neutrons, recent developments in accelerator technology have made possible the construction of pulsed neutron sources, providing steady, intermittent neutron beams.

Name	Location	Type
HFBR	Brookhaven National Laboratory, USA	Reactor
HFIR	Oak Ridge National Laboratory, USA	Reactor
HFR	Institute Laue Langevin, France	Reactor
IPNS	Argonne National Laboratory, USA	Spallation
ISIS	Rutherford-Appleton Laboratory, UK	Spallation
LANSE	Los Alamos National Laboratory, USA	Spallation
NBS	National Institute of Standards and Technology, USA	Reactor
MURR	University of Missouri, USA	Reactor
OWR	Los Alamos National Laboratory, USA	Reactor
ORR	Oak Ridge National Laboratory, USA	Reactor

Table 1 **Some neutron sources.**

Within nuclear reactors, neutrons are a primary product of nuclear fission. By controlling the rate of the nuclear reactions, one controls the flux of neutrons and provides a steady supply of neutrons. For a diffraction analysis, a narrow band if neutron wavelengths is selected (fixing λ) and the angle 2θ is varied to scan the range of d values.

Pulsed sources use a process called *spallation*. If a high-energy pulsed beam of protons impinges upon a heavy metal target, a rather complex series of nuclear excitations and relaxations results in a burst of high-energy neutrons from the target. Since the spallation process occurs rapidly (in less than 1 μs), a pulsed source can be operated at 30–120 Hz (30–120 pulses per second), providing a steady, intermittent source of neutrons. Then, rather than select a narrow wavelength range for diffraction analysis, the full spectrum of neutron wavelengths are used in the diffraction experiment. Neutron wavelengths vary predictably with momentum according to the equation

$$\lambda = \frac{ht}{ml} \tag{2}$$

where λ is the neutron wavelength, h is Planck's constant, t is time, m is the neutron mass, and l is the neutron flight path. By noting the time of flight of a detached neutron, its wavelength can be deduced.

The difference between the neutron diffraction experiment performed at a steady-state (reactor) or a pulsed source are illustrated in Figure 3. Despite the

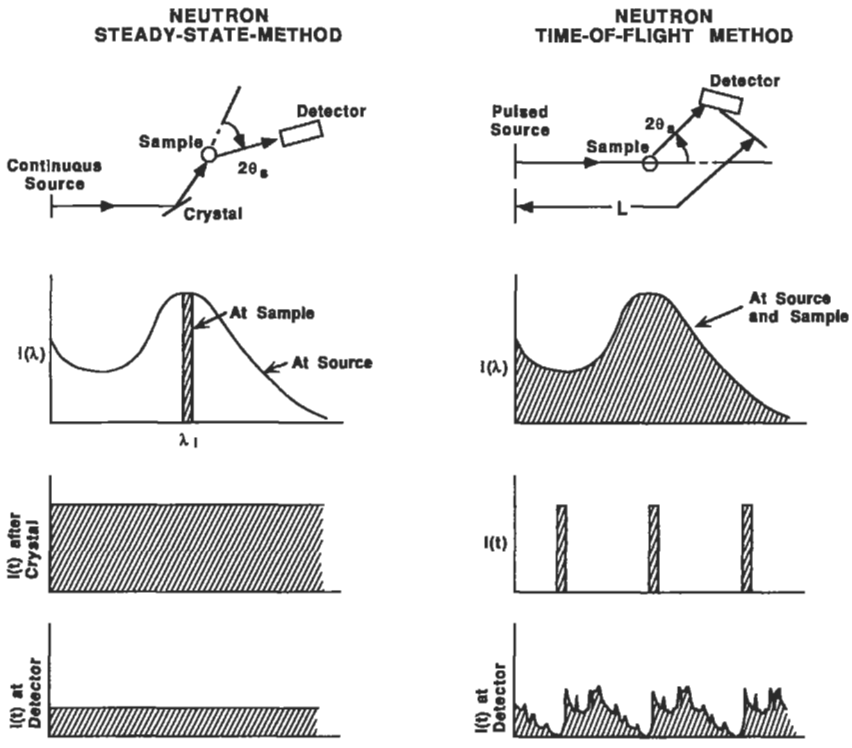

Figure 3 **Comparison of nuclear reactor and pulsed spallation sources. For reactor sources (steady-state method), a narrow band of wavelengths is selected with a monochromator crystal and the scattering angle ($2\theta_s$) is varied to scan *d* spacings. Pulsed sources (time-of-flight method) use almost the entire available neutron spectrum, fix the scattering angle ($2\theta_s$), and simultaneously detect a neutron while determining its time of flight.**

major differences in the design and instrumentation, the quality of data and usable neutron intensities for the two sources are comparable. Some currently available neutron sources are listed in Table 1.

Use of Neutron Diffraction

Neutron diffraction is particularly well suited for use in

1 Structural investigations of heavy metal oxides (particularly when oxygen positions or occupancies are important)
2 *In-situ* analysis
3 Determinations of magnetic ordering in crystalline materials
4 Bulk analysis of physically large pieces.

Specific examples of the first and third uses are given below.

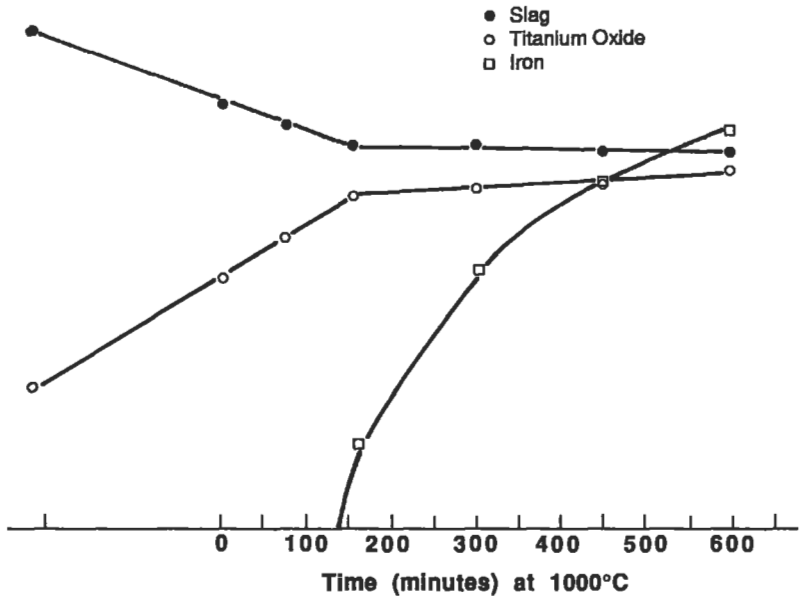

Figure 4 **Plot of time-resolved decomposition of titanium-enriched slags as extracted from neutron diffraction data collected at 1000° C.**

In-Situ Analysis

Figure 4 illustrates the results of neutron diffraction data collected at 1000° C as a function of time. The data were collected during the thermal degradation of commercial titanium slags.[1] The slags are produced by a smelting process used to enrich the titanium content of ilmenite ore. The purpose of the diffraction experiment was to determine the growth of particular undesirable phases as a function of time at the decomposition temperature of the slag. In addition to providing information about the type and number of phases that appeared during decomposition, it was also highly desirable to obtain detailed structural information about the newly appearing phases, as well as the changing nature of the decomposing phase.

Each set of data points for a particular time in Figure 4 represents a neutron diffraction pattern collected in a 15-minute period. Each of the data sets was analyzed to quantify the phases present, determine the identities and locations of metal atoms within each oxide phase, and accurately measure the unit cell parameters (an indication of the phase composition). Examples of the raw neutron diffraction data from which the useful data given in Figure 4 have been extracted are given in Figure 5. In Figure 5, peaks due to two of the decomposition products, titanium oxide (TiO_2) and iron metal, are marked; examination of the figure illustrates the utility of diffraction data. The appearance of Bragg peaks due to newly formed phases are clearly distinguished from those of the parent compound.

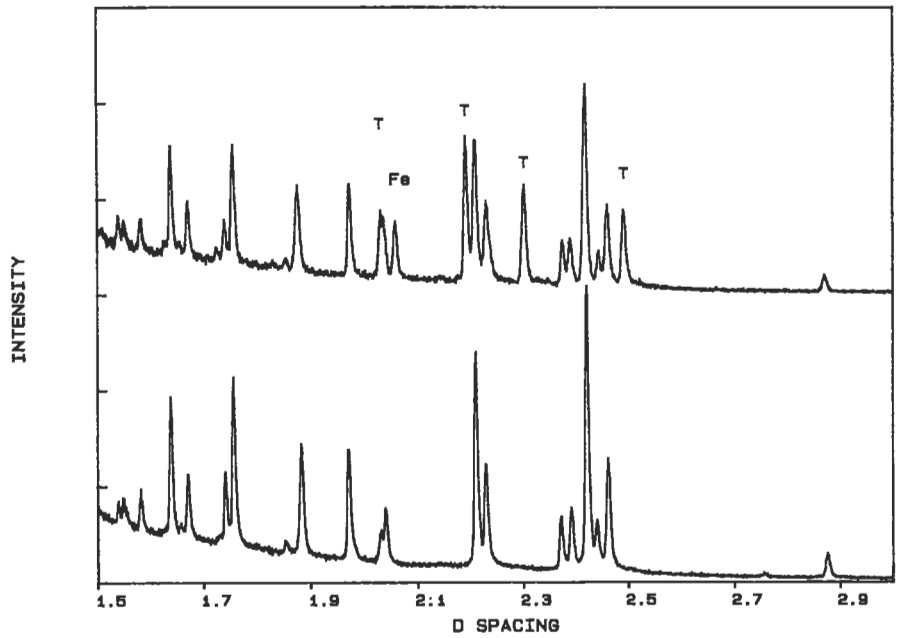

Figure 5 **Raw diffraction data at the start (bottom) and completion (top) of the *in-situ* decomposition of slag experiments. Most of the peaks in the pattern are due to the parent slag phase. Bragg peaks due to titanium oxide (T) and iron metal (Fe) are marked.**

It can be seen from Figure 4 that two distinct reaction pathways describe the decomposition of the slag. From the beginning of decomposition up to approximately 150 min, a pathway that results in the production of titanium oxide dominates the chemistry. After this initialization period, the decomposition rate diminishes greatly, and metallic iron formation becomes important. Additional features of the decomposition (not illustrated in Figures 4 and 5) also resulted from analysis of the neutron diffraction data. The most important of these was that a specific atomic arrangement of the titanium and iron atoms was required before decomposition could occur, and that a certain minimum temperature was required for this rearrangement. Knowledge of this atomic shifting and the temperature required for its occurrence led to an understanding of the maximum temperature above which slags would begin to decompose.

Superconducting Oxides

One of the most exciting and perhaps unexpected discoveries in science within the last decade has been the observation of superconductivity (the complete absence of resistivity to electric current) in metal oxides at temperature ≤ 90 K. This tempera-

ture range is particularly important because it can be reached with readily available liquid nitrogen (77 K). Important structural features of metal oxide superconductors have been revealed largely by the application of neutron diffraction.

In a sense, a superconductor is an insulator that has been doped (contains random defects in the metal oxide lattice).[2] Some of the defects observed via neutron diffraction experiments include metal site substitutions or vacancies, and oxygen vacancies or interstituals (atomic locations between normal atom positions). Neutron diffraction experiments have been an indispensable tool for probing the presence of vacancies, substitutions, or interstituals because of the approximately equal scattering power of all atoms.

Studies of the superconducting phase $YBa_2Cu_3O_{7-x}$ exemplify this point. *In-situ* neutron diffraction analysis revealed that during the synthesis of this material (above 900° C) oxygen vacancies occur and that the composition at this temperature is close to $YBa_2Cu_3O_6$ ($x = 1$). Upon cooling in an oxygen atmosphere, the oxygen vacancies are filled to form the superconducting material $YBa_2Cu_3O_{7-x}$, raising the average oxidation state of the copper above +2. These results are presented in Figure 6. The figure shows that as the temperature is reduced from about 600° C to room temperature, the occupancy of one oxygen site—O1, located at (0,½,0) in the unit cell—approaches 100%, while that of a second oxygen atom—O5, located at (½,0,0)—tends toward 0. It has been shown that the superconductivity of this metal oxide is a function of its oxygen content, and therefore a function of the partial occupancies of O1 and O5.

An advantage enjoyed by neutron diffraction over X-ray diffraction was outlined in the introduction. Since X rays are scattered by electrons, X-ray diffraction data from the $YBa_2Cu_3O_{7-x}$ system are mainly sensitive to the metal atom positions and occupancies, and much less sensitive to the oxygen atoms. Hence the key features of the $YBa_2Cu_3O_{7-x}$ superconductor—oxygen vacancies—would not be apparent from the analysis of X-ray diffraction data. However, since neutrons are scattered approximately equally by all atoms, a neutron diffraction experiment is very sensitive to the structural features of importance in this system. An additional advantage of neutrons over X rays in work of this type is the need for *in-situ* data. To understand the role of oxygen vacancies in the $YBa_2Cu_3O_{7-x}$ system, it was necessary to collect diffraction data over a wide range of temperatures and oxygen partial pressures. The greater penetrating nature of the neutron is well suited to the use of special equipment required for these types of experiments, since the neutrons can pass right through such equipment.

Another example of the use of neutron diffraction to understand the role of atomic vacancies in producing a superconducting metal oxide phase is work that has been performed on $Ba_{0.6}K_{0.4}BiO_3$. This work demonstrates that at the synthesis temperature (700° C), under the proper conditions, oxygen vacancies are created to allow the formation of the parent phase with bismuth largely in the +3 oxidation state. The presence of the vacancies allows the incorporation of potassium in the

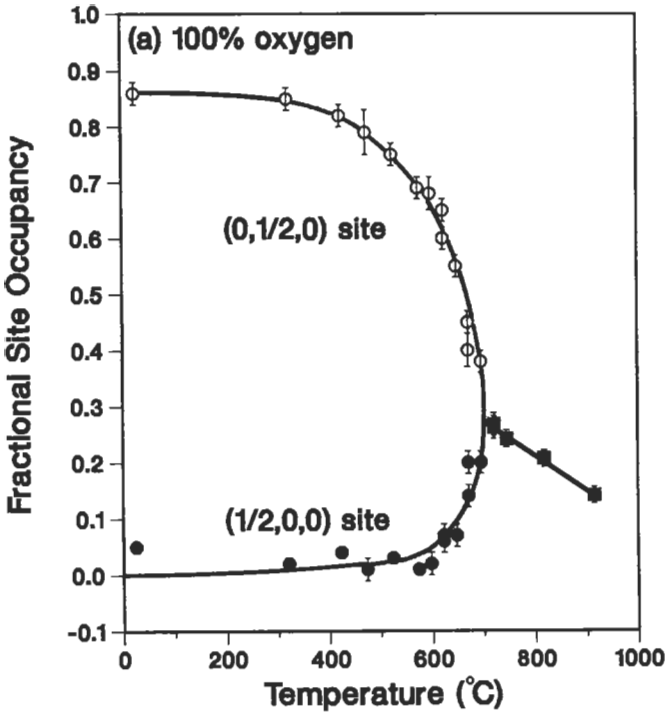

Figure 6 **Site occupancies for two of the oxygen atoms (O1 and O5) in the $YBa_2Cu_3O_{7-x}$ superconductor as a function of temperature. The site occupancies resulted from an analysis of *in-situ* neutron diffraction data. Reprinted by permission from Jorgensen and Hinks.[2]**

structure. As the temperature is reduced, the oxygen vacancies are filled, and because the potassium atoms lose their mobility at lower temperatures, the overall structure remains intact, producing a phase with bismuth in an unusually high oxidation state.

Magnetic Thin Films

Neutron diffraction is a powerful probe of the magnetic structure and ordering in magnetic thin films. Rare earth thin films and multilayers (materials having a repeating modulation in chemical composition) present an interesting class of materials, and neutron diffraction has been instrumental in elucidating their magnetic structure.[7] For multilayers of Dy, Er, and Gd alternating with Y, neutron diffraction has shown that the magnetic order is propagated through the intervening nonmagnetic Y layers. For DY-on-Y multilayers, it was found that the magnetically ordered state was an incommensurate helical antiferromagnetic state. That is, the magnetic moments in each basal plane are ferromagnetically aligned, but somewhat

rotated between adjacent basal planes. Although this is similar to bulk Dy, the temperature dependence of the rotation, or turn, angle is different than in bulk Dy. It would be difficult or impossible to determine this microscopic information using a technique other than neutron diffraction. While the thickness of the magnetic films in these measurements was ~4000 Å, rare earth films as thin as ~500 Å and transition metal oxide films as thin as ~5000 Å can be analyzed. For multilayers, neutron measurements at very low angles are also useful in characterizing magnetic order; these are described in the article on neutron reflectivity.

Conclusions

Historically, due to the general unavailability of neutron sources, neutron diffraction has been a rather esoteric technique. Fortunately, the neutron users' community has expanded over the last decade, and concerted programs encouraging new users at many facilities have extended the use of the technique into the general scientific community. While neutron diffraction may never become a routine analytical tool, data collection times for studies requiring its use usually can be found

It has been shown that neutron diffraction offers the same kind of information that other diffraction techniques offer, namely atomically resolved structure determination and refinement, as well as phase identification and quantitation. Other uses not described herein include residual stress measurements, and determinations of average particle sizes for crystalline materials. The major advantage of neutrons with respect to the more readily available X rays lies in the greater penetrating power of the neutron, and the approximately equal scattering ability of nuclei. These features make neutron diffraction the proper choice when *in-situ* measurements, bulk penetration, or site occupancies of atoms are required.

Related Articles in the Encyclopedia

XRD and Neutron Reflectivity

References

1 Details of the thermal decomposition of commercial slags can be found in R. G. Teller, M. R. Antonio, A. Grau, M. Guegin, and E. Kostiner. *J. Solid State Chem.* 1990.

2 Discussion of neutron diffraction studies of superconductors was largely taken from J. D. Jorgensen and D. G. Hinks. *Neutron News.* **24,** 1, 1990.

3 For further discussion of neutron sources, see R. B. Von Dreete. *Reviews in Mineralogy. Volume 20: Modern Powder Diffraction.* **333,** 20, 1990.

4 For a detailed discussion of pulsed neutron sources, see J. D. Jorgensen and J. Faber. *ICANS-II, Proceedings of the Sixth International Collaboration*

on Advances in Neutron Sources. Argonne National Laboratory technical report ANL-82-80, 1983.

5 Important concepts in neutron diffraction can be found in G. E. Bacon. *Neutron Diffraction.* Clarendon Press, third edition, 1975.

6 The general principles of diffraction can be found in numerous books, for example, B. D. Cullity. *Elements of X-Ray Diffraction.* Addison-Wesley, New York, second edition, 1978.

7 For a review, see J. J. Rhyne, R. W. Erwin, J. Borchers, M. B. Salamon, R. Du, and C. P. Flynn. *Physica B.* **159,** 111, 1989.

11.2 Neutron Reflectivity

THOMAS P. RUSSELL

Contents

Introduction

Neutron reflectivity offers a means of determining the variation in concentration of a material's components as a function of depth from the surface or at an interface buried within the material, with a resolution of ~1 nm. Because of the large neutron contrast between hydrogen and deuterium, one may highlight a particular component through isotopic labeling with deuterium without substantially altering the thermodynamics of the system. This, however, normally means that reflectivity studies are relegated to the investigation of model systems that are designed to mimic the behavior of the system of interest.

Other technique—for example, dynamic secondary ion mass spectrometry or forward recoil spectrometry—that rely on mass differences can use the same type of substitution to provide contrast. However, for hydrocarbon materials these methods attain a depth resolution of approximately 13 nm and 80 nm, respectively. For many problems in complex fluids and in polymers this resolution is too poor to extract critical information. Consequently, neutron reflectivity substantially extends the depth resolution capabilities of these methods and has led, in recent years, to key information not accessible by the other techniques.

An additional advantage to neutron reflectivity is that high-vacuum conditions are not required. Thus, while studies on solid films can easily be pursued by several techniques, studies involving solvents or other volatile fluids are amenable only to reflectivity techniques. Neutrons penetrate deeply into a medium without substantial losses due to absorption. For example, a hydrocarbon film with a density of $1 g/cm^3$ having a thickness of 2 mm attenuates the neutron beam by only 50%. Consequently, films several μm in thickness can be studied by neutron reflectivity. Thus, one has the ability to probe concentration gradients at interfaces that are buried deep within a specimen while maintaining the high spatial resolution. Materials like quartz, sapphire, or aluminum are transparent to neutrons. Thus, concentration profiles at solid interfaces can be studied with neutrons, which simply is not possible with other techniques.

The single most severe drawback to reflectivity techniques in general is that the concentration profile in a specimen is not measured directly. Reflectivity is the optical transform of the concentration profile in the specimen. Since the reflectivity measured is an intensity of reflected neutrons, phase information is lost and one encounters the age-old inverse problem. However, the use of reflectivity with other techniques that place constraints on the concentration profiles circumvents this problem.

The high depth resolution, nondestructive nature of thermal neutrons, and availability of deuterium substituted materials has brought about a proliferation in the use of neutron reflectivity in material, polymer, and biological sciences. In response to this high demand, reflectivity equipment is now available at all major neutron facilities throughout the country, be they reactor or spallation sources.

Basic Principles

Considering Figure 1, radiation incident on a surface (light, X rays, or neutrons) will be reflected and refracted at the interface between the two media provided there is a difference in the index of refraction. In the case of neutrons and X rays, the refractive index of a specimen is slightly less than unity and, to within a good approximation, is given by

$$n = 1 - \delta + i\beta \tag{1}$$

The imaginary component of the refractive index is associated with absorption. In general, the absorption for thin films is not significant and, consequently, β can be ignored. However, for materials containing the elements Li, B, Cd, Sm, or Gd, where the absorption coefficient is large, β must be taken into account and the refractive index is imaginary.

The real component of the neutron refractive index δ is related to the wavelength λ of the incident neutrons, the neutron scattering length (a measure of the extent to which neutrons interact with different nuclei), the mass density and the atomic

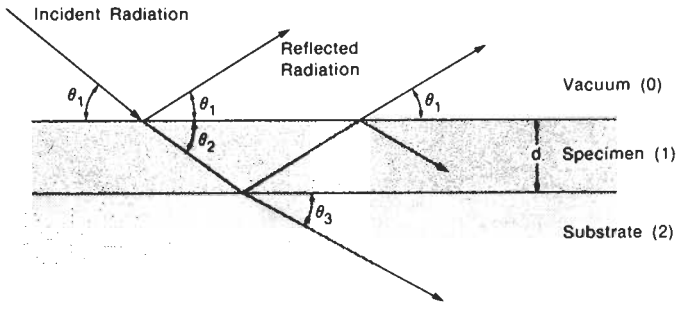

Figure 1 **Schematic diagram of the neutron reflectivity measurement with the neutrons incident on the surface and reflected at an angle θ_1 with respect to the surface. The angle θ_2 is the angle of refraction. The specimen in this case is a uniform film with thickness *d*, on a substrate.**

number of the components comprising the specimen. Values of the neutron scattering length for all the elements and their isotopes are tabulated.[1] The neutron scattering length does not vary systematically with the atomic number. This is shown in Figure 2. As can be seen, isotopes of a given element can have markedly different neutron scattering lengths while two different elements with vastly different atomic numbers can have similar scattering lengths. In fact, the difference between the proton and the deuteron provides one of the largest differences and offers the most convenient manner of labeling materials for neutron reflectivity studies.

In Table 1 values of δ are given for some common inorganic and organic compounds. First notice that δ is on the order of 10^{-6}. Therefore, the neutron refractive index differs from unity by only a small amount. With the exception of H_2O and

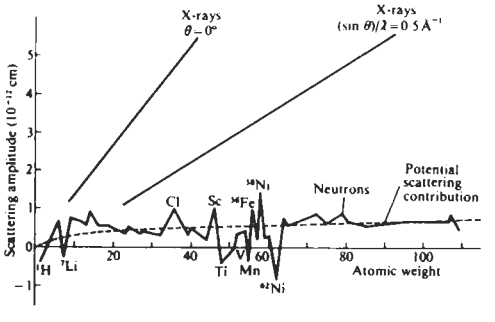

Figure 2 **Variations in the neutron scattering amplitude or scattering length as a function of the atomic weight. The irregularities arise from the superposition of resonance scattering on a slowly increasing potential scattering. For comparison the scattering amplitudes for X rays under two different conditions are shown. Unlike neutrons, the X-ray case exhibits a monotonic increase as a function of atomic weight.**

Substance	Chemical formula	ρ (g/cm^3)	Σb_i (10^{12} cm)	$\delta^\dagger$ (10^{12} cm)	$\theta_C^\dagger$ (10^3)	$k_C^\dagger$ ($Å^{-1}$)
Water	H_2O	1.00	–0.168	–0.212	—	—
	D_2O	1.11	1.914	2.41	2.19	0.0089
Benzene	C_6H_6	0.879	1.74	0.445	0.943	0.0038
		0.946	7.99	2.043	2.021	0.0082
Polyethylene	$(CH_2)_x$	0.95	–0.08	–0.128	—	—
	$(CD_2)_x$	1.08	1.99	3.067	2.477	0.0101
Polystyrene	$(C_8H_8)_x$	1.0	2.32	0.509	1.01	0.0041
	$(C_8D_8)_x$	1.08	10.656	2.336	2.16	0.0088
Silicon oxide	SiO_2	2.32	1.58	1.371	1.655	0.0067
Silicon	Si	2.32	0.42	0.791	1.26	0.0051

†Calculated for neutrons with $\lambda = 1.5$ Å.

In this list, ρ is the mass density, Σb_i is the sum of scattering lengths of the atoms comprising the molecule, δ is the real part of the refractive index, θ_C is the critical angle, and k_C is the critical neutron momentum.

Table 1 **Important neutron reflection parameters for some common materials.**

polyethylene $(CH_2)_x$, $\delta > 0$ and therefore $n < 1$. The refractive index for air or vacuum is unity. From Snell's law it is easy to show that total external reflection occurs when the incidence angle, θ, is less than $(2\delta)^{1/2}$. Above this critical angle θ_C the reflectivity decreases and the manner of this decrease contains all the information pertinent to gradients in the concentration normal to the surface of the specimen.

Consider the simple case shown in Figure 1, where we have a uniform film on a substrate with a thickness of 50 nm. For demonstration purposes the film is a deuterated polystyrene on a silicon substrate. The reflectivity profile obtained from such a specimen is shown in Figure 3. The reflectivity is plotted as a function of the neutron momentum k_{z0}, which is proportional to $(\sin\theta)/\lambda$, where the subscript $z0$ indicates the z-direction (normal to the surface) in vacuum (0), λ is the wavelength and θ is the incidence angle. Using k_{z0} reduces data to a scale that is independent of λ and θ used in an experiment. Below θ_C total external reflection is seen, then the reflectivity is seen to decay with a series of oscillations. The oscillations, characterizing the film thickness, arise from interferences between neutrons reflected at the air and substrate interfaces. In general the higher the frequency of the oscillations, the thicker the specimen.

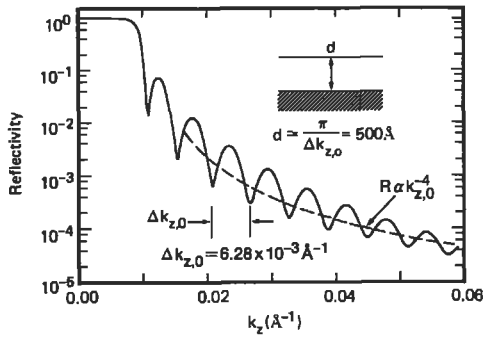

Figure 3 **A calculated reflectivity profile for a perdeuterated polystyrene film with a thickness of 50 nm on a silicon substrate. The calculation was for a specimen where the interfaces between the specimen and air and the specimen and the substrate were sharp. This causes the reflectivity on average (shown by the dashed line) to decrease in proportion to k_{z0}^{4} or θ^{-4}. The separation distance between the minima of the oscillations directly yields the thickness of the specimen, as shown.**

On average, the reflectivity decays in proportion to θ^{-4} or k_{z0}^{-4} since both interfaces are sharp. However, if either surfaces is rough, then marked deviations are seen and the reflectivity is damped by a factor of $\exp\{-2k_{z0}^{2}\sigma^{2}\}$, where σ is the root-mean-square roughness. Thus, the reflectivity is very sensitive to surface roughness and to concentration gradients at interfaces.

The reflectivity for this simple case can be extended readily to more complex situations where there are concentration gradients in single films or multilayers comprised of different components. Basically the reflectivity can be calculated from a simple recursion relationship that effectively reduces any gradients in composition to a histogram representing small changes in the concentration as a function of depth. Details on this can be found in the literature cited.[2–4]

For specimens where gradients in the magnetic moment are of interest, similar arguments apply. Here, however, two separate reflectivity experiments are performed in which the incident neutrons are polarized parallel and perpendicular to the surface of the specimen. Combining reflectivity measurements under these two polarization conditions in a manner similar to that for the unpolarized case permits the determination of the variation in the magnetic moments of components parallel and perpendicular to the film surface. This is discussed in detail by Felcher et al.[5] and the interested reader is referred to the literature.

The neutron's momentum can be varied by changing λ or θ. With a fixed wavelength the angle of incidence can be changed by rotating the sample. This, typically, is the situation one encounters at steady state nuclear reactors, where a specific wavelength of the neutrons emanating from the reactor core is selected with a monochromator. Such facilities are available at the Oak Ridge National Laboratory, the National Institute of Standards and Technology, and the Brookhaven National Laboratory in the United States, and at the Institut Laue Langevin (Grenoble) and the Kernforschungsanlage facility (Jülich) in Europe. Here, a collimated beam of monochromatic neutrons impinges on the surface of the specimen at an angle θ and a detector is placed behind a set of slits at an angle 2θ with respect to the incident beam (this is termed the specular condition). The geometry is shown in Figure 1. Both the specimen and detector are rotated synchronously at θ and 2θ, respectively, to measure the reflected neutrons as a function of θ. Since λ is known, θ is equivalent to k_{z0}. Normalization of the reflected intensity against the incident intensity yields the reflectivity directly.

Spallation sources are an alternative means of generating neutrons. As opposed to a reactor source, a target is bombarded with pulses of high-energy charged particles, for example, protons on a uranium target. Neutrons with a broad energy or wavelength distribution are generated at the target, passed through a cold moderator, and delivered into the experimental area. The velocity of a neutron is proportional to its energy and inversely proportional to its wavelength. Thus, knowing the time at which the pulse of protons hits the target and the distance to the source, we have that the time for a neutron to reach the detector is proportional to its wavelength. Hence the term *time of flight* is used. Argonne National Laboratory and the Los Alamos National Laboratory in the United States, and Rutherford Appleton Laboratories in Europe have reflectometers that are based on this principle.

At spallation sources, k_{z0} is varied by wavelength because pulsed streams of neutrons with a range of wavelengths are delivered onto the specimen surface at an angle θ. Knowing the incident distribution of wavelengths and measuring the distribution of wavelengths reflected at an angle θ with respect to the surface furnishes directly the reflectivity of the specimen. The beauty of the time-of-flight measurements is that there are no moving parts to the reflectometer. Unlike the fixed-wavelength spectrometers, with time-of-flight spectrometers exactly the same area of the specimen is measured for all values of k_{z0}. This is very important if the sample is not uniform across its surface.

One of the key advantages to time-of-flight reflectometers comes in the measurement of fluid surfaces. Simply delivering the neutrons onto the fluid surface at a fixed angle (without moving the specimen) and detecting the reflected neutrons yields the reflectivity profile.

Specimen Considerations

The measurements of concentration gradients at surfaces or in multilayer specimens by neutron reflectivity requires contrast in the reflectivity for the neutrons. Under most circumstances this means that one of the components must be labeled. Normally this is done is by isotopic substitution of protons with deuterons. This means that reflectivity studies are usually performed on model systems that are designed to behave identically to systems of more practical interest. In a few cases, however (for organic compounds containing fluorine, for example) sufficient contrast is present without labeling.

Neutron reflectivity measures the variation in concentration normal to the surface of the specimen. This concentration at any depth is averaged over the coherence length of the neutrons (on the order of 1 μm) parallel to the surface. Consequently, no information can be obtained on concentration variations parallel to the sample surface when measuring reflectivity under specular conditions. More importantly, however, this mandates that the specimens be as smooth as possible to avoid smearing the concentration profiles.

Typically specimens for reflectivity measurements are prepared on flat, smooth, rigid substrates. For example, these substrates can be polished fused silica, quartz, or silicon. It is important, however, that the substrates be thick to avoid distortions of the specimen when mounted in the reflectometer. Any curvature or bowing will increase the divergence of the incident beam and result in a deterioration of the resolution.

The substrates usually range from 5 cm to 10 cm in diameter. Such large specimens are required because experiments are performed at small angles of incidence and it is necessary to intercept the entire beam with the specimen. For example, consider the projection of a beam 0.1 mm in size onto a specimen at an angle of 2 mrad (~ 0.11°). Under such conditions, the incident beam will illuminate 5 cm of the surface. For specimens that are dominantly protonated, the critical angle is smaller and the projection is even larger. The large diameter of the specimens places stringent requirements on the sample's preparation, but it is not difficult to achieve uniformity for such large specimens and the preparation is routine.

Examples

The first studies on the use of neutron reflectivity appeared approximately 20 years ago and dealt with the investigation of Langmuir-Blodgett films. Surprisingly, the utility of the technique for the investigation of other materials was not fully realized and its use and availability virtually ceased. Only in the last four years has there been a resurgence of the use of neutron reflectivity, and now there are reflectometers available throughout the United States and abroad. This resurgence stems from the focus of the scientific community on surface and interfacial phenomena. In

fact, interfacial behavior of polymeric materials has provided a rich area where the true power of neutron reflectivity has been brought to bear. There is no question, though, that surface and interfacial problems in other organic, inorganic and magnetic materials can be studied by neutron reflectivity. These areas have been discussed at length in the literature.[4–6] For the purposes of illustration, we shall focus on two specific problems in polymers that demonstrate the capabilities of reflectivity.

In numerous applications of polymeric materials multilayers of films are used. This practice is found in microelectronic, aeronautical, and biomedical applications to name a few. Developing good adhesion between these layers requires interdiffusion of the molecules at the interfaces between the layers over size scales comparable to the molecular diameter (tens of nm). In addition, these interfaces are buried within the specimen. Aside from this practical aspect, interdiffusion over short distances holds the key for critically evaluating current theories of polymer diffusion. Theories of polymer interdiffusion predict specific shapes for the concentration profile of segments across the interface as a function of time. Interdiffusion studies on bilayered specimen comprised of a layer of polystyrene (PS) on a layer of perdeuterated (PS) d-PS, can be used as a model system that will capture the fundamental physics of the problem. Initially, the bilayer will have a sharp interface, which upon annealing will broaden with time.

Neutron reflectivity is ideally suited to this problem, since concentration profiles can be resolved on the nanometer level and since, for an infinitely sharp interface, Rk_{z0}^{4} will approach asymptotically a constant value. In addition, neutron reflectivity is nondestructive and multiple experiments can be performed on the same specimen. Figure 4 shows a plot of Rk_{z0}^{4} as a function of k_{z0} for a bilayer of protonated polystyrene (h-PS) on a layer of, d-PS prepared as described. Near the critical angle, Rk_{z0}^{4} reaches a maximum value then decreases, approaching an average constant value of 3×10^{-10} Å^{-4}. Thus, the initial interface is sharp. Evident in the reflectivity profile are a series of oscillations with frequencies characterizing the thicknesses of the h-PS and d-PS layers and the combined thickness. The solid line in the figure corresponds to a reflectivity profile calculated assuming a 67.5-nm layer of h-PS on an 185-nm layer of d-PS with an interfacial width of only 1 nm.

Upon heating the bilayer for two minutes at 105.5°C, where the glass transition temperature of PS is 100° C, interdiffusion occurs. As shown by the plot of Rk_{z0}^{4} versus k_{z0} (offset by a factor of 10), the overall features of the reflectivity remained unchanged with the exception that the asymptotic limit decreased to 1.4×10^{-10} Å^{-4}. The solid line in the figure was calculated using the layer thicknesses mentioned above, but the interface was characterized now by an error function with a width of 3 nm. Combining these measurements with others at longer times and at different temperatures proved that reptation (the movement of the polymer along its own contour), coupled with rapid motions of the polymer chain between entanglements, quantitatively describes the interdiffusion process.

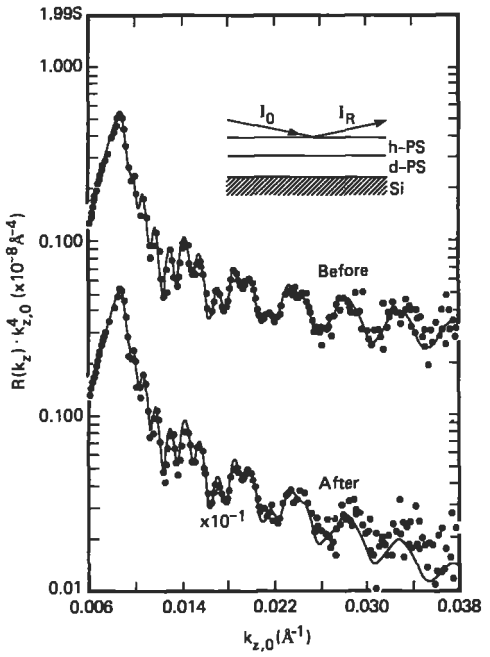

Figure 4 **The reflectivity multiplied by k_{z0}^4 as a function of k_{z0} for a bilayer of normal polystyrene on perdeuterated polystyrene before and after heating at 105.5° C for 2 minutes. The data is plotted in this manner since for sharp interfaces Rk_{z0}^4 is a constant at large k_{z0}.**

The second example deals with symmetric diblock copolymers. Diblock copolymers are finding widespread use as compatibilizing agents, adhesion promoters and surface-modifying agents. Diblock copolymers are comprised of two chemically different polymer chains covalently bonded together at one point. In cases where the length of the blocks are equal, lamellar domains of each component comparable to the size of the polymers are formed at the junction points between the two blocks at the interfaces. The chemical differences between the blocks causes a preferential segregation of one of the components to the air or substrate interfaces, in thin films, which leads to an orientation of the lamellar domains parallel to the film surface.

Figure 5 shows the neutron reflectivity profile of a diblock copolymer of PS and polymethylmethacrylate (PMMA), where the PS block is labeled with deuterium. The reflectivity profile exhibits five clearly resolved maxima characterizing the period of the lamellar microdomains. A high-frequency oscillation, characteristic of the total specimen thickness, is also seen. Note that below the critical angle ($k_{z0} \sim 0.006$ Å^{-1}) the reflectivity is not unity, due to the finite size of the specimen. The solid line in the figure was calculated using the scattering length density or concentration profile shown in the inset. This model is comprised of PS layers having a

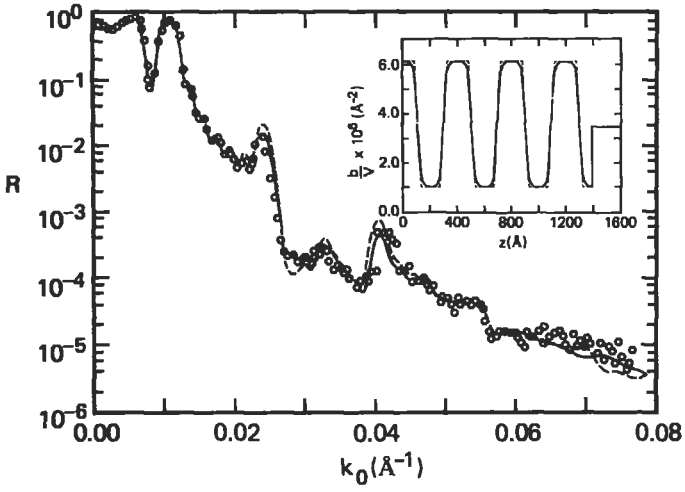

Figure 5 **Neutron reflectivity of a symmetric diblock copolymer of PS and PMMA annealed at 160° C for 24 hours under vacuum. The inset contains scattering length density profiles used to calculate the corresponding reflectivity profiles. The solid line represents the reflectivity profile calculated using the scattering length density (or concentration) profile as a function of distance *z* from the air surface where a hyperbolic tangent describes the interface between the layers. The dashed line was calculated using a linear gradient between the microdomains. This small change, as can be seen, produces a significant change in the reflectivity profile.**

thickness of 21 nm and PMMA layers having a thickness of 18.8 Å. The interface between the layers is characterized by a hyperbolic tangent function with an effective width of 5.0 ± 0.3 nm. At the air–copolymer and copolymer–substrate interfaces, the adjacent PS and PMMA layers, respectively, are one-half the thickness of those seen in the bulk. The major importance of these results comes in the precision to which the interface between the PS and PMMA layers can be determined. This far exceeds that possible by other techniques. To emphasize this, a second reflectivity profile (shown as the dashed line) was calculated assuming a linear gradient at the interface. While the differences in the segment density profiles are small, the differences in the reflectivity profile are pronounced, clearly demonstrating the details resolvable by neutron reflectivity.

Conclusions

Neutron reflectivity provides a depth resolution of ~1 nm and fills an important gap in the resolution between X-ray photoelectron spectroscopy and ion-beam techniques. In this regard, neutron reflectivity promises to play a decisive role in the investigation of solid materials. Equally important is the fact that reflectivity meas-

urements can be used to study liquid specimens, which is not possible with other techniques requiring high vacuum. Many problems on the swelling and dissolution of materials with low molecular weight solvents, the adsorption of materials onto a surface or at the liquid–air interface or liquid–liquid interface, or transport through membranes in solution on specific interactions of materials with interfaces in the presence of a solvent can be addressed by neutron reflectivity.

Theoretical and experimental advances are being made on understanding reflectivity under nonspecular conditions. This permits the determination of correlations in composition parallel to the specimen's surface thereby adding a new dimension to existing capabilities. Studies under nonspecular conditions promise to be quite important in elucidating systems containing inhomogeneities parallel to the sample's surface. From this will stem a quantitative characterization of surface roughness, curvature of interfaces, capillary waves, and the configurations and conformations of molecules at surfaces and interfaces.

Related Articles in the Encyclopedia

Neutron Diffraction

References

1 G. E. Bacon. *Neutron Diffraction.* (3rd edition) Clarendon Press, Oxford, 1975.

2 O. S. Heavens. *Optical Properties of Thin Solid Films.* Butterworths, London, 1955.

3 J. Lekner. *Theory of Reflection.* Nighoff, Dordrecht, 1987.

4 T. P. Russell. *Mat. Sci. Rep.* **5,** 171, 1990.

5 G. P. Felcher, R. O. Hilleke, R. K. Crawford, J. Haumann, R. Kleb, and G. Ostrowski. *Rev. Sci. Instrum.* **58,** 609, 1987.

6 J. Penfold, R .C. Ward, and W. G. Williams. *J. Phys.* **E20,** 1411, 1987.

11.3 NAA

Neutron Activation Analysis

TIM Z. HOSSAIN

Contents

Introduction

Neutron activation analysis (NAA) is a sensitive analytical technique for measuring trace impurities in a wide variety of materials. NAA has been used for trace analysis in polymers, biological materials, and geological and environmental samples. It has been used successfully to study the role of trace elements in Alzheimer's Disease by measuring impurities in human brain tissue. Trace impurities in air particulates have been measured to correlate emissions from fossil fuel power plants. Since there are many excellent texts describing the applications of NAA in these fields, the present article will be devoted entirely to NAA of semiconductor materials. NAA is highly suited for elements of interest to semiconductor manufacturing. For example, NAA can detect Cu, Zn, and Au in Si with detection limits of 7×10^{12}, 1×10^{12}, and 3×10^{7} atoms/cc, respectively.[1] Results obtained using this method usually provide bulk concentrations, however, surface-sensitive measurements can be made by combining chemical etching with NAA. The method is not suitable for depth profiling, such as can be done with SIMS. Neither is there a capability for

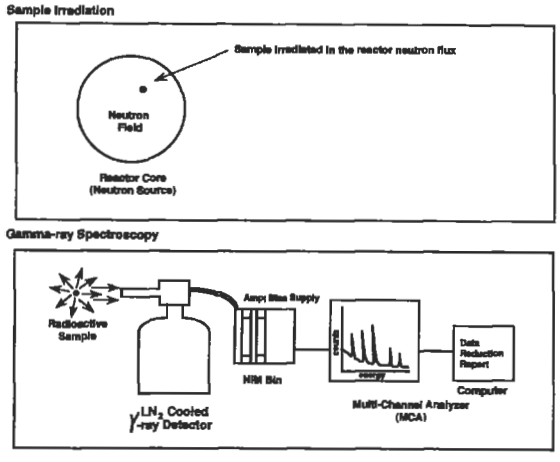

Figure 1 **Schematic of Neutron Activation Analysis.**

microspot analysis. The strength of NAA lies in its ability to perform quantitative bulk analysis at sub-ppb levels. Almost two-thirds of the elements in the periodic table can be analyzed easily. Light elements like H, N, O, or F are not suitable candidates for NAA, and Al and Cl can be analyzed only with high detection limits in a Si matrix.

Most of the transition elements that are of primary interest in the semiconductor industry such as Fe, Cr, Mn, Co, and Ni, can be analyzed with very low detection limits.[1] Second to its sensitivity, the most important advantage of NAA is the minimal sample preparation that is required, eliminating the likelihood of contamination due to handling. Quantitative values can be obtained and a precision of 1–5% relative is regularly achieved. Since the technique measures many elements simultaneously, NAA is used to scan for impurities conveniently.

It is applicable to plastic packaging materials, where purities with respect to mobile ions, such as Cl and Na, can be checked. In addition, α-particle precursors, such as U and Th, can be determined in solid plastics with sub-ppb detection limits.

Basic Principles

Irradiation

All NAA experiments are conducted in two steps: irradiation and counting as indicated in Figure 1. Samples are made radioactive by placing them in a neutron field. Typically a research nuclear reactor provides the necessary neutron flux. Elements present in the sample capture neutrons, and often become radioactive isotopes. This part of the experiment is known as irradiation. A typical irradiation in a reac-

tor core position (where the neutron flux is high) may last about 1–7 days. The total integrated neutron dose received, in general, determines the detection limits obtained. Typical research reactors are capable of delivering $1–5 \times 10^{13}$ neutrons/cm^2 s.

It is important to note that the neutron capture probability, called the *cross section* σ, is vastly different for various elements. Excellent sensitivity for Au is due largely to its high cross section (σ = 100 barns; 1 barn = 1×10^{-24} cm^2). Other elements, such as Pb, have low cross sections and much poorer detection limits.

Elements with multiple stable isotopes may produce several radioisotopes that can be measured to assure the accuracy of the analysis. For example, Zn has five stable isotopes.[2] The isotope ^{64}Zn will produce the radioisotope ^{65}Zn, and ^{68}Zn will produce the radioisotope ^{69}Zn. Both of these radioisotopes can provide an independent measurement of the Zn concentration and therefore can be used to check the consistency and quality of the analysis. On the other hand, ^{66}Zn will produce ^{67}Zn, which is nonradioactive and therefore cannot be used in NAA.

At the end of the irradiation, the samples are withdrawn from the reactor and γ-ray spectroscopy is carried out. Most often the laboratory performing the γ-ray spectroscopy is located in a different city, in which case the samples are shipped and the reactor serves as a neutron source only. Many reactors also have γ-ray spectroscopy capability so that measurements can be made at the reactor site as well.

Counting, or γ-Ray Spectroscopy

All radioactive isotopes decay with a characteristic half-life. For example, ^{59}Fe decays with a half-life of 45 days, while ^{64}Cu decays with a half-life of 12.6 hours. As a result of the decay, signature high-energy photons or γ rays are emitted from a given radioisotope. Thus, ^{59}Fe emits two prominent γ rays at 1099 and 1292 keV, ^{24}Na emits at 1368 and 2754 keV, and ^{65}Zn emits at 1115 keV. Compilations of γ rays used in NAA can be found in γ-ray tables.

The emission of γ rays follows, in the majority of cases, what is known as β decay. In the β-decay process, a radionuclide undergoes transmutation and ejects an electron from inside the nucleus (i.e., not an orbital electron). For the purpose of simplicity, positron and electron capture modes are neglected. The resulting transmutated nucleus ends up in an excited nuclear state, which promptly relaxes by giving off γ rays. This is illustrated in Figure 2.

For the purpose of the activation analysis these high-energy γ rays are used or counted in a spectroscopy mode to obtain concentration values. Energy-dispersive spectroscopy of the γ rays is accomplished using a solid state detector constructed of high-purity single-crystal germanium. The detector is connected via a preamplifier and an amplifier to a multichannel analyzer (MCA). The sample holder and the detector are contained in a lead-shielded chamber. The radioactive sample serves as the γ-ray source and is placed in a convenient geometry in front of the detector. The response time of the detector must be fast enough so that each γ ray entering the

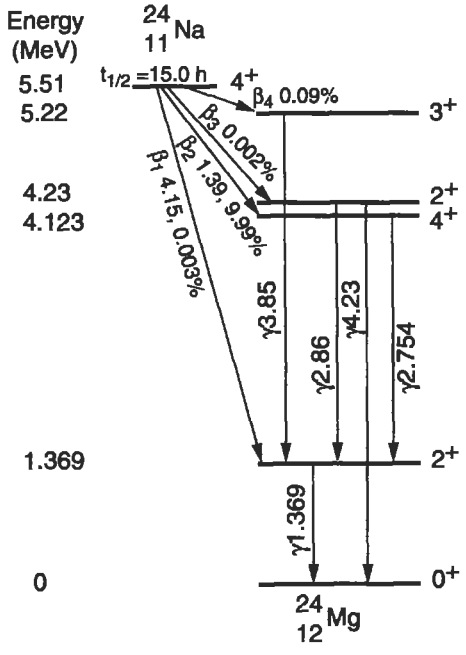

Figure 2 **Decay scheme of ^{24}Na. The transition energies are in MeV.[9]**

detector volume is processed as a single event. The γ rays are sorted by energy and counted in appropriate channels of the MCA. A spectrum is generated of intensity (counts) versus energy of the γ rays. While the energy of the γ ray is used to identify the element, the number of counts provides a measure of the concentration.

NAA can achieve ultralow detection limits for most impurities in a Si or SiO_2 matrix because Si itself has a low neutron capture cross section and produces radioisotopes having short half-lives. The only significant radioisotope, ^{31}Si, has a half-life of 2:6 hours. Radioactivity from this isotope, although initially intense, will therefore be reduced to a negligible intensity after 2–3 days. The impurities of interest, such as Cr and Fe, have long half-lives. By delaying the start of the count, a high signal-to-noise ratio is obtained. This indicates that for other matrices, such as HgCdTe and GaAs, in which both the cross sections and the half-lives are not as favorable, NAA is rendered less practical. On the other hand, organic matrices, such as polymers and biological samples, can be conveniently analyzed because the light elements C, H, O, and N have low neutron capture cross sections.

Sample Requirements

Size requirements are limited by packaging considerations for neutron irradiation. Typically, polyethylene or quartz containers are used to contain the sample in the reactor core. For example, Si wafers are cleaved into smaller pieces and flame sealed

in high-purity quartz vials (e.g., suprasil quartz) for irradiation. The size of the irradiation port in the reactor core will typically limit the size of the polyethylene or quartz container. All handling is done wearing talc-free gloves and using white plastic tweezers. (Avoid the green-colored Teflon-coated stainless steel variety.) An intact full wafer (e.g., having a diameter of 4") usually cannot be inserted into an irradiation port of high neutron intensity ($> 1 \times 10^{13}$ neutrons/ (cm^2 s), since most ports have diameters of less than 4" It is desirable to perform NAA before any metallization steps (with Ti, W, or Cu, for example) have been carried out. This avoids a high intensity of radiation from the irradiated thin metal layer. Other important considerations are the dopants present in the wafer. Both As and Sb become readily activated (with half-lives 26.7 hours for As, and 64 hours and 60 days for the two radioisotopes of Sb), so that samples implanted with high doses of As and Sb ($> 1 \times 10^{14}$ atoms/ cm^2) are not suitable for NAA. However, B and P dopants do not pose problems during NAA.

Quantification

NAA is a quantitative method. Quantification can be performed by comparison to standards or by computation from basic principles (parametric analysis). A certified reference material specifically for trace impurities in silicon is not currently available. Since neutron and γ rays are penetrating radiations (free from absorption problems, such as those found in X-ray fluorescence), matrix matching between the sample and the comparator standard is not critical. Biological trace impurities standards (e.g., the *National Institute of Standards and Technology Standard Reference Material,* SRM 1572 Citrus Leaves) can be used as reference materials. For the parametric analysis many instrumental factors, such as the neutron flux density and the efficiency of the detector, must be well known. The activation equation can be used to determine concentrations:

$$A = \frac{\text{cps}}{\varepsilon_d \varepsilon_p} = n\phi f\sigma (1 - e^{-\lambda t_i}) e^{-\lambda t_d}$$

where A is the activity in disintegrations/ second; *cps* stands for counts/ second in a given photopeak (i.e., a specific γ ray); ε_d is the efficiency of the detector for the photopeak; ε_p is the photon fraction (i.e., the number of γ rays/ 100 decays); n is the number of atoms of the element of interest (unknown); ϕ is the isotopic abundance of the target; f is the neutron flux density; σ is the neutron cross section; λ is the decay constant for the radioisotope; t_i is the length of irradiation; and t_d is the time elapsed since the end of irradiation.

Applications

NAA has been used to determine trace impurities in polysilicon, single-crystal boules, silicon wafers, and processed silicon, as well as plastics used for packaging.[3–5]

Element	Polysilicon (ppba)	Single crystal (ppba)
Ag	< 0.00130	< 0.00110
As	0.02400	0.00810
Au	0.00007	0.00005
Ba	Not identified	Not identified
Co	< 0.00640	< 0.00490
Cr	0.0520	< 0.00600
Cs	< 0.00040	< 0.00020
Cu	0.00590	0.00730
Fe	< 0.44000	< 0.25000
Ga	Not identified	Not identified
Hf	< 0.00021	< 0.00015
In	< 0.01800	< 0.05900
Mo	< 0.01300	Not identified
Na	Not identified	0.62000
Rb	< 0.01100	< 0.01000
Sb	< 0.00040	< 0.00250
Sc	< 0.00005	< 0.00004
Ta	< 0.00008	< 0.00010
Zn	< 0.00150	< 0.00110
Zr	< 0.1800	< 0.13000

Table 1 Comparison of NAA data for polysilicon and single-crystal CZ silicon.[3]

An example of an analysis done on polysilicon and single-crystal Czochralski silicon (CZ) is shown in Table 1. As can be seen, polysilicon, which was used to grow the crystal, is "dirtier" than the CZ silicon. This is expected, since segregation coefficients limit the incorporation of each element into the crystal boule during the crystal growth process. All values shown in the table are from bulk analysis. Table 2 shows NAA data obtained in an experiment where surface analysis was accom-

Impurity surface (4 μ)	Concentration (atoms/cc)	Epitaxial film (> 4 μ)
Au	1×10^{13}	1×10^{12}
Cu	7×10^{14}	6×10^{13}
Na	3×10^{15}	7×10^{13}

Table 2 **Surface concentrations of impurities on a Si wafer, as measured by NAA.[4]**

plished by using chemical etching following irradiation. The wafer surface is usually etched with a HF/HNO_3 / glacial acetic acid mixture and a 2–3 μm layer is etched off by controlling the length of the etching time. Both the etched wafer and the etchant solution are then measured. Many etchants developed for wafer fabrication can be used for these measurements. Table 3 shows results obtained from NAA of plastic packaging materials. Low detection limits from U and Th are particularly noteworthy.

Although the majority of NAA applications have been in the area of bulk analysis, some specialized uses need to be mentioned. One such unique application is the measurement of phosphorus in thin films (about 5000 Å) of phosphosilicate (PSG) or borophosphosilicate (BPSG) glasses used in VLSI device fabrication. In this case,

Impurity element	PVDF (4 qualities) (ppbw)	PVI (5 lots) (ppbw)
Au	0.1–0.3	0.005–0.05
Cu	65–100	110–1800
Cr	< 10–70	50–300
Co	< 2–15	5–10
Ca	80,000–130,000	Not analyzed
Cd	Not analyzed	1000–3000
Mn	6–26	25–80
Na	1700–4200	300–1000
W	0.3–1	1–4
U	0.3–0.7	< 0.1–0.5
Th	< 0.05–0.3	< 0.06–0.7

Table 3 **Selected impurity concentrations in plastics, as measured by NAA.[5]**

a PSG or a BPSG wafer (usually a pilot wafer) is activated and ^{31}P (stable) is converted to ^{32}P (14.2-day half-life). After a week of decay, the major radioactivity remaining is due to ^{32}P, which can be counted with a gas flow counter.[6]

Another application involves the measurement of copper via the radioisotope ^{64}Cu (12.6-hour half-life). Since ^{64}Cu decays by electron capture to ^{64}Ni ($^{64}Cu \rightarrow {}^{64}Ni$), a necessary consequence is the emission of X rays from Ni at 7.5 keV. By using X-ray spectrometry following irradiation, sensitive Cu analysis can be accomplished. Because of the short range of the low-energy X rays, near-surface analytical data are obtained without chemical etching. A combination of neutron activation with X-ray spectrometry also can be applied to other elements, such as Zn and Ge.

Neutron activation also has been combined with accelerator mass spectrometry and has been demonstrated to have part-per-billion sensitivities for bulk nitrogen analysis in silicon. This combination was also used to obtain depth profile of Cl in silicon semiconductors.[7]

Limitations

NAA cannot be used for some important elements, such as aluminum (in a Si or SiO_2 matrix) and boron. The radioactivity produced from silicon directly interferes with that from aluminum, while boron does not produce any radioisotope following neutron irradiation. (However, an in-beam neutron method known as *neutron depth profiling* can be used to obtain boron depth profiles in thin films.[8]) Another limitation of NAA is the long turn-around time necessary to complete the experiment. A typical survey measurement of all impurities in a sample may take 2–4 weeks.

For matrices other than silicon, such as GaAs, InSb, AlGaAs, and InP, it is difficult to measure trace elements because the activity from the matrix is intense and long-lived. In these cases, laborious radiochemical separation techniques are employed to measure impurities.

Conclusions

NAA is well suited for Si semiconductor impurities analysis. The sensitivity and the bulk mode of analysis make this an important tool for controlling trace impurities during crystal growth or for monitoring cleanliness of various processing operations for device manufacturing. It is expected that research reactors will serve as the central analytical facilities for NAA in the industry. Since reactors are already set up to handle radioactive materials and waste, this makes an attractive choice over installing individual facilities in industries.

Related Articles in the Encyclopedia

XRF, PIXE, Dynamic SIMS, and NRA

References

1 M. L. Verheijke, H. J. J. Jaspers, and J. M. G. Hanssen. *J. Radioanal. Nucl. Chem.* **131,** (1) 197, 1989.

2 F. W. Walker, J. R. Parrington, and F. Feiner. *Chart of the Nuclides, 14th Edition.* General Electric Company, 1989, pp. 26–27.

3 M. Domenici, P. Malinverni, and M. Pedrotti. *J. Cryst. Growth.* **75,** 80, 1986.

4 G. B. Larrabee and J. A. Keenan. *J. Electrochem. Soc.* **118,** (8) 1351, 1971.

5 E. W. Haas and R. Hofmann. *Solid State Electronics.* **30,** (3) 329, 1987.

6 P. M. Zeitzoff, T. Z. Hossain, D. M. Boisvert, and R. G. Downing. *J. Electrochem. Soc.* **137,** (12) 3917, 1990.

7 P. Sharma, P. W. Kubik, H. E. Gove, U. Fehn, R. T. D. Teng, S. Datar, and S. Tullai-Fitzpatrick. *Annual Report NSRL–360.* University of Rochester, Rochester, 1990.

8 R. G. Downing, J. P. Lavine, T. Z. Hossain, J. B. Russell, and G. P. Zenner. *J. Appl. Phys.* **67,** (8) 3652, 1990.

9 *Nuclear and Radiochemistry.* (Third edition) John Wiley & Sons, New York, 1981.

11.4 NRA

Nuclear Reaction Analysis

DANIELE J. CHERNIAK AND W.A. LANFORD

Contents

Introduction

Nuclear reaction analysis (NRA) is used to determine the concentration and depth distribution of light elements in the near surface (the first few μm) of solids. Because this method relies on nuclear reactions, it is insensitive to solid state matrix effects. Hence, it is easily made quantitative without reference to standard samples. NRA is isotope specific, making it ideal for isotopic tracer experiments. This characteristic also makes NRA less vulnerable than some other methods to interference effects that may overwhelm signals from low abundance elements. In addition, measurements are rapid and nondestructive.

NRA can be highly sensitive, with typical detection limits of 10^{19} atoms/cm^3, depending on the reaction involved. Depth resolutions typically range from a few nm to tens of nm, and lateral resolutions down to a few μm can be achieved with microbeams.

An especially significant application of NRA is the measurement of quantified hydrogen depth profiles, which is difficult using all but a few other analytical techniques. Hydrogen concentrations can be measured to a few tens or hundreds of parts per million (ppm) and with depth resolutions on the order of 10 nm.

As NRA is sensitive only to the nuclei present in the sample, it does not provide information on chemical bonding or microscopic structure. Hence, it is often used in conjunction with other techniques that do provide such information, such as ESCA, optical absorption, Auger, or electron microscopy. As NRA is used to detect mainly light nuclei, it complements another accelerator-based ion-beam technique, Rutherford backscattering (RBS), which is more sensitive to heavy nuclei than to light nuclei.

NRA has a wide range of applications, including use in investigations of metals, glasses, and semiconductor materials, and in such diverse fields as physics, archaeology, biology, and geology.

Basic Principles

General[1]

A beam of charged particles (an *ion* beam) with an energy from a few hundred keV to several MeV is produced in an accelerator and bombards a sample. Nuclear reactions with low-Z nuclei in the sample are induced by this ion beam. Products of these reactions (typically p, d, t, ^{3}He, α particles, and γ rays) are detected, producing a spectrum of particle yield versus energy. Many (p, α) reactions have energies that are too low for efficient detection. In these cases, the associated γ rays are detected instead. Important examples are:

$$^{19}F + p \rightarrow {}^{16}O + \alpha + \gamma$$

$$^{15}N + p \rightarrow {}^{12}C + \alpha + \gamma$$

These reactions may be used, respectively, to profile ^{19}F and ^{15}N, using incident proton beams, or to profile hydrogen, using incident beams of ^{19}F and ^{15}N.

NRA exploits the body of data accumulated through research in low-energy nuclear physics to determine concentrations and distributions of specific elements or isotopes in a material. Two parameters important in interpreting NRA spectra are reaction Q values and cross sections.

Q values are the energies released in specific nuclear reactions and are used to calculate the energies of particles resulting from the reaction. Reactions with large positive Q values are most suitable for NRA. Table 1 presents Q values for a number of nuclear reactions. More comprehensive compilations of these data exist.[2] Reaction cross sections have also been measured as functions of incident ion energy and beam–detector angle. As particle yields are directly proportional to reaction cross sections, this information permits the experimenter to select an incident beam energy and detector angle that will maximize sensitivity. In addition, concentrations can be calculated directly from particle yields without reference to standards if the cross sections are accurately known. Similarly, the yields and energies of γ rays

Isotope	Q (MeV)	Isotope	Q (MeV)	Isotope	Q (MeV)
		(p, α) reactions			
^{7}Li	17.347	^{6}Li	4.022	^{9}Be	2.125
^{11}Be	8.582	^{18}O	3.970	^{31}P	1.917
^{19}F	8.119	^{37}Cl	3.030	^{27}Al	1.594
^{15}N	4.964	^{23}Na	2.379	^{17}O	1.197
				^{10}B	1.147
		(d, α) reactions			
^{3}He	18.352	^{31}P	8.170	^{13}C	5.167
^{10}B	17.819	^{11}B	8.022	^{32}S	4.890
^{6}Li	22.360	^{15}N	7.683	^{18}O	4.237
^{7}Li	14.163	^{9}Be	7.152	^{30}Si	3.121
$^{14}N_{(\alpha 0)}$	13.579	^{25}Mg	7.047	^{16}O	3.116
^{19}F	10.038	^{23}Na	6.909	^{26}Mg	2.909
^{17}O	9.812	^{27}Al	6.701	^{24}Mg	1.964
$^{14}N_{(\alpha 1)}$	9.146	^{29}Si	6.012	^{28}Si	1.421
		(d, p) reactions			
^{3}He	18.352	^{17}O	5.842	^{30}Si	4.367
^{10}B	9.237	^{31}P	5.712	^{26}Mg	4.212
^{25}Mg	8.873	^{27}Al	5.499	^{12}C	2.719
$^{14}N_{(p0)}$	8.615	^{24}Mg	5.106	^{16}O	1.919
^{29}Si	8.390	^{6}Li	5.027	^{18}O	1.731
^{32}S	6.418	^{23}Na	4.734	$^{14}N_{(p5)}$	1.305
^{28}Si	6.253	^{9}Be	4.585	^{11}B	1.138
^{13}C	5.947	^{19}F	4.379	^{15}N	0.267

Table 1 ***Q* values for nuclear reactions induced by protons and deuterons on some light isotopes.[14]**

resulting from nuclear reactions have been determined. Mayer and Rimini[3] include reaction cross sections and γ yields as functions of the incident ion energy for a number of light elements, as well as a table of γ-ray energies as a function of ion energy for (p, γ) reactions involving many low- to medium-Z elements.

Resonant Profiling

Resonant profiling uses beam energies near narrow isolated resonances of relevant nuclear reactions to determine the depth distribution of elements in a sample. A good illustration of this technique is hydrogen profiling using the reaction ^{1}H (^{15}N, αγ) ^{12}C, with a resonance energy of 6.385 MeV. The expression in the previous sentence is a shorthand form used to describe the nuclear reaction. The term before the parentheses is the nucleus of interest (the species to be profiled). The first term in parentheses is the incident particle. The remaining components are the products of the reaction. Those in parentheses (after comma) are the species that are detected. In this case, the target is bombarded with ^{15}N ions and the yield of characteristic γ rays resulting from the reaction of the ^{15}N with ^{1}H is measured. When the energy of the incident beam E_0 is equal to the resonance energy E_R, the γ yield is proportional to the hydrogen content on the sample surface. If the beam energy is raised, the resonance energy is reached at a depth x, where the energy lost by the incident ions in traversing a distance x in the target is $E_0 - E_R$. The γ yield is now proportional to the hydrogen concentration at x. This is illustrated schematically in Figure 1. Contributions to the γ yield due to H in the surface region are greatly diminished, as the nuclear reaction cross section is large near the resonance energy but drops by several orders of magnitude for energies more than a few keV away. By continuing to raise the incident beam energy, one can profile further into the sample.

In this case, converting the γ yield-versus-incident beam energy profile to a concentration-versus-depth profile is straightforward. This is because the energy loss rate of the ^{15}N ions with depth (dE/dx) is large with respect to variations in individual ion energies after they have traveled a distance x in the material. In practice, these energy *straggling* effects can be neglected.

The depth scale is determined simply by

$$x = \frac{E_0 - E_R}{dE/dx} \tag{1}$$

The detected yield is a function of the concentration of the element being profiled, the resonance cross section, the detector efficiency, and dE/dx. To be specific,

$$\rho = KY(dE/dx) \tag{2}$$

where ρ is the concentration of the element being profiled, Y is the reaction yield (e.g., number of γ rays per microcoulomb of ^{15}N beam), dE/dx is the energy loss

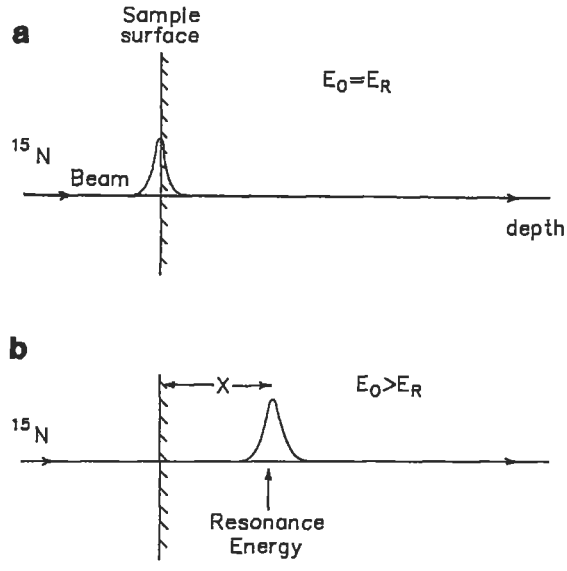

Figure 1 **Schematic illustration of resonant profiling technique. In (a), the incident ^{15}N beam is at resonance energy (E_R) and hydrogen on sample surface is detected. With higher beam energies (b), hydrogen is measured at depth x, where $x \cong (E_0-E_R)/(dE/dx)$.**

rate of the incident ion in the target, and K is the *calibration* constant for the particular nuclear reaction and analysis chamber, a parameter independent of the material being analyzed.

Determination of concentration profiles from the raw data can be more complicated when protons are used as the incident particles. The energy loss (dE/dx) is smaller for protons and straggling effects are more important. The observed profile $N(E_0)$ is a convolution of the actual concentration profile $C(x)$ with a depth resolution function $q_0(x, E_0)$, which broadens with increasing x roughly as $\sqrt{x}$. Hence, resolution deteriorates with depth. However, near-surface resolution for resonant profiling may be on the order of tens of Å.

Nonresonant Profiling

When reaction cross sections are sufficiently large over an extended energy range, the entire depth profile may be obtained using a single incident beam energy. This is referred to as nonresonant profiling.

An example of this technique is the profiling of ^{18}O using the reaction ^{18}O (p, α) ^{15}N. Figure 2 shows the cross section of this reaction as a function of

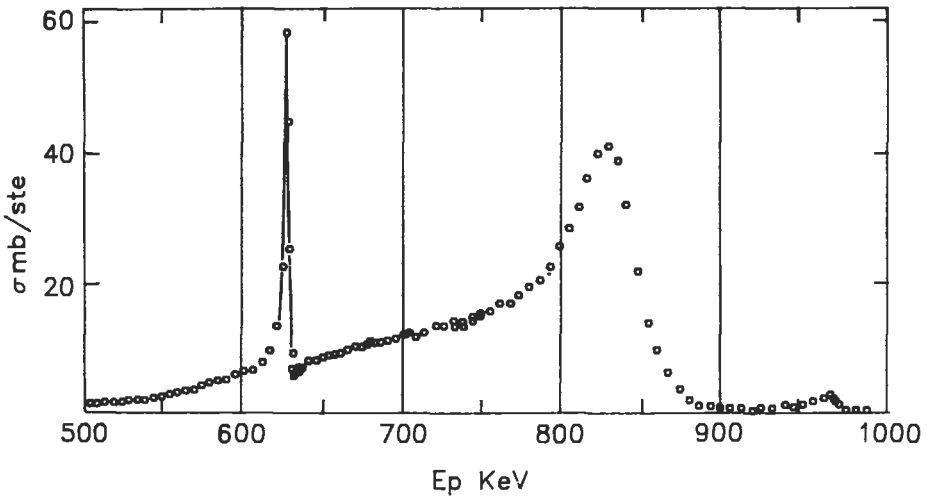

Figure 2 **Cross section versus incident proton energy for the ^{18}O (p, α) ^{15}N reaction, with a beam-detector angle of 165°.[14]**

incident proton energy, illustrating the large and smoothly varying cross section in the vicinity of 800 keV. It should be noted that ^{18}O also can be profiled using the resonant technique, employing the sharp resonance at 629 keV.

For nonresonant profiling, a sample is bombarded with protons at a suitable energy and the α particles resulting from the reaction of the protons with ^{18}O are detected. A spectrum of α particles over a range of energies is collected, representing contributions from ^{18}O at various depths in the material. The α spectra are converted to depth profiles in a manner analogous to that outlined above for H profiling. However, it must be noted that in this case not only the incoming protons, but also the outgoing α particles, lose energy traveling through the sample (unlike γ rays). The detected energy for ^{18}O on the sample surface can be calculated from the kinematics, using the incident proton energy, the angle between the incident beam and the particle detector, and the Q value for the reaction (3.97 MeV in this case). As they travel deeper into the sample, the protons lose energy. When these protons interact with the ^{18}O, the resultant α particles have a lower energy than those from the surface. The particles lose additional energy as they travel out of the material, so α particles from a certain depth will have a characteristic energy. This is illustrated schematically in Figure 3. To construct the depth scale from this information, the rate of energy loss for protons and α particles in the material must be known. This information is tabulated for most elements,[4] and values for compound targets can be calculated by weighting the elemental contributions according to their abundances in the material.

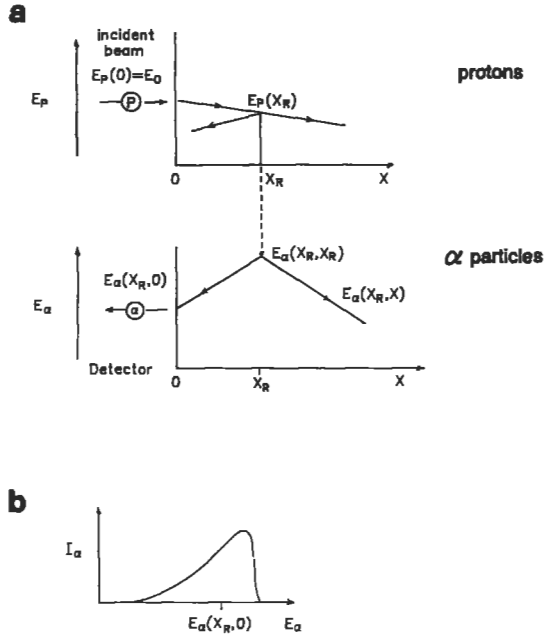

Figure 3 **Schematic illustration of nonresonant profiling technique. Incident protons lose energy with increasing depth x in the sample (a). At depth x_R, a proton with energy $E_p(x_R)$ induces a nuclear reaction with a target atom of ^{18}O, producing an α particle of energy $E_\alpha(x_R, x_R)$. The α particle loses energy as it travels out of the sample, resulting in the detected energy $E_\alpha(x_R, 0)$. The distribution of ^{18}O in the sample at various depths (b) results in a spectrum of α yield I_α versus detected alpha energy E_α.**

The number of detected α particles corresponding to a particular depth is a function of the detector solid angle, the total proton flux delivered to the sample, the reaction cross section at the appropriate energy, and the concentration of ^{18}O at that depth. Once again, the observed profile is a convolution of the actual concentration profile with a *spreading* or energy resolution function that takes into consideration such factors as the energy spread of the incident beam, proton and α-particle straggling in the sample, and detector resolution. Concentrations may be determined without reference to standards if these experimental parameters are known.

In nonresonant profiling, the silicon surface barrier detectors that detect the products of the nuclear reaction may also detect signals from incident ions that have been backscattered from the sample. Figure 4 shows an α particle spectrum from the reaction ^{18}O (p, α) ^{15}N, along with the signal produced by backscattered protons. The yield of backscattered particles (which is proportional to Z^2) may overwhelm the electronics in the detecting system, resulting in a pileup that greatly

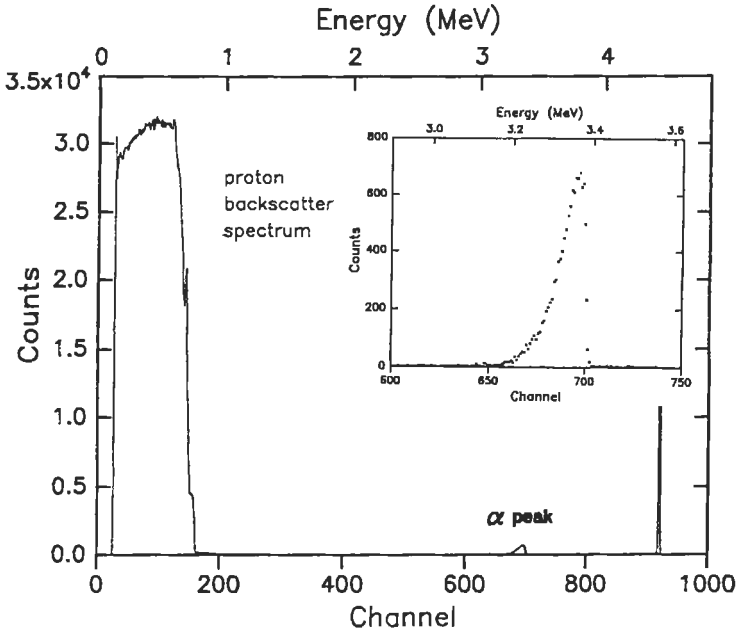

Figure 4 **Spectrum of ^{18}O diffusion in the mineral olivine ($(Mg, Fe)_2 SiO_4$) taken using nonresonant profiling technique with the reaction ^{18}O (p, α) ^{15}N. Both the α particles resulting from the nuclear reaction and backscattered protons are collected. Inset shows expanded region of the spectrum, where α yield indicates diffusion of ^{18}O into the material.**

reduces sensitivity. This difficulty is compounded by the fact that cross sections for nuclear reactions are generally much smaller than backscattering cross sections. A solution to this problem is to shield the detector with a thin-film absorber (such as Mylar). The absorber (of appropriate thickness) stops the backscattered incident ions, while permitting the higher energy ions from the nuclear reaction to pass into the detector. However, the presence of an absorbing material degrades depth resolution, since additional energy spreading occurs as the ions travel through the absorber to the detector. Because of this trade-off between depth resolution and sensitivity, the experimenter should weigh the usefulness of absorbers in each case. In ^{18}O profiling, for example, absorbers would be needed when profiling tantalum oxide, but may not be required during analysis of glasses and minerals having low-Z matrices, where ion backscattering is much reduced.

Characteristics

Selectivity and Quantification

Because of the nature of the technique, NRA is sensitive only to the nuclei present in the sample. While this characteristic prohibits obtaining direct information on

chemical bonding in the material, it makes analyses generally insensitive to matrix effects. Therefore, NRA is easily made quantitative without reference to standard samples.

Since NRA focuses on inducing specific nuclear reactions, it permits selective observation of certain isotopes. This makes it ideal for tracer experiments using stable isotopes. Generally, there are no overlap or interference effects because reactions have very different Q values, and thus different resultant particle energies. This permits the observation of species present at relatively low concentrations. A good example is oxygen: ^{16}O and ^{18}O can be resolved unambiguously, as they are detected with completely different nuclear reactions; e.g., ^{16}O (d, p) ^{17}O, and ^{18}O (p, α) ^{15}N.

Resolution

Depth resolution in NRA is influenced by a number of factors. These include energy loss per unit depth in the material, straggling effects as the ions travel through the sample, and the energy resolution of the detection system.

As earlier discussed, the dominant factor in the near-surface region is the particle detection system. For a typical silicon surface barrier detector (15-keV FWHM resolution for ^4He ions), this translates to a few hundred Å for protons and 100–150 Å for ^4He in most targets. When γ rays induced by incident heavy ions are the detected species (as in H profiling), resolutions in the near-surface region may be on order of tens of Å. The exact value for depth resolution in a particular material depends on the rate of energy loss of incident ions in that material and therefore upon its composition and density.

In many cases, depth resolution in the near-surface region also can be improved by working at a grazing angle attained geometrically by tilting the sample. This increases the path length required to reach a given depth below the surface, which in turn produces an increase in effective depth resolution.

Straggling effects become more dominant further into the sample. They are most pronounced with proton beams, because the ratio of energy straggling to energy loss decreases with increasing ion mass. For protons, these effects may be quite substantial; for example, depth resolutions in excess of 1000 Å are typical for 1-MeV protons a few μm into a material.

With the use of a microbeam, lateral resolution with NRA on the order of several μm is possible. However, because of the small beam currents obtainable with microbeam systems, sensitivity is limited and reactions with relatively large cross sections are most useful. Only a few laboratories perform microbeam measurements.

Sensitivity

The sensitivity of NRA is affected by reaction cross sections, interfering reactions and other background effects. Hence, it is impossible to make general statements as

to what sensitivities for NRA will be without considering the specific reactions and sample materials involved in each case. However, sensitivities on the order of 10–100 ppm are common.

Other Considerations

Sample Requirements

The maximum sample size is limited only by the design of the sample chamber. Typically, samples up to several cm in diameter can be accommodated. A diameter of a few mm is generally the lower limit because high-energy ion beams focused through standard beam optics are on the order of a few mm in diameter; however, microbeam setups permit the use of samples an order of magnitude smaller.

Nonconducting samples require special consideration. The incident ion beam causes a buildup of positive charge on the sample surface. Discharging of the sample may create noise in the spectrum collected by surface barrier detectors. In addition, the presence of accumulated positive charge on the sample may affect the accuracy of current integration systems, making it difficult to determine the exact beam dose delivered to the target. This problem may be obviated by flooding the sample surface with electrons to compensate for the buildup of positive charge or by depositing a thin layer of conducting material on the sample surface. If the latter option is chosen, the slowing down of ions in this layer must be considered when calculating depth scales. In addition, care must be taken to select a material that will not experience nuclear reactions that could interfere with those of the species of interest.

Accidental Channeling Effects

When analyzing single-crystal samples, the experimenter should be aware that accidental channeling may occur. This happens when the sample is oriented such that the ion beam is directed between rows or planes of atoms in the crystal, and generally results in reduced yields from reactions and scattering from lattice atoms. Such effects may be minimized by rotating the target in such a way to make the direction of the beam on the target more random. In some cases, the use of molecular ions (i.e. H_2^+ or H_3^+ instead of H^+) can also reduce the probability of accidental channeling. The molecular ions break up near the sample surface, producing atomic ions that repel and enter the material with more random trajectories, reducing the likelihood of channeling.

However, when deliberately employed, channeling is a powerful tool that may be used to determine the lattice positions of specific types of atoms or the number of specific atoms in interstitial positions (out of the lattice structure). Further information on this technique is available.[5]

Simulation Programs for NRA

There are a number of computer codes available[6, 7] to simulate and assist in the evaluation of NRA spectra. Most of these programs are similar to or compatible with the RBS simulation program RUMP. These programs require the input of reaction cross sections as a function of incident ion energy for the appropriate beam–detector geometry. The user interactively fits the simulation to the data by adjusting material parameters, such as the bulk composition and the depth distribution of the component being profiled. SPACES[6] is designed to deal specifically with narrow resonances (e.g., ^{27}Al (p, γ) ^{28}Si at 992 keV) and their associated difficulties, while SENRAS[7] is useful in many other cases.

Applications

In this section, a number of applications for NRA are presented. As this is not a review article, the following is only a sampling of the possible uses of this powerful technique. The reader interested in information on additional applications is directed to the proceedings of the Ion Beam Analysis Conferences[8] and those from the International Conferences on the Application of Accelerators in Research and Industry,[9] among other sources.

Hydration Studies of Glass

A combination of nuclear reactions have been used in studies of the processes involved in the hydration and dissolution of glass. Lanford et al.[10] investigated the hydration of soda-lime glass by measuring Na and H profiles. The profiles (Figure 5) indicate a depletion of sodium in the near-surface region of the glass and a complementary increase in hydrogen content. The ratio of maximum H concentration in the hydrated region and Na concentration in unhydrated glass is 3:1, suggesting that ionic exchange between H_3O^+ and Na^+ is occurring.

Residual Carbon in Ceramic Substrates

Multilayer ceramic substrates are used as multiple chip carriers in high-performance microelectronic packaging technologies. These substrates, however, may contain residual carbon which can adversely affect mechanical and electrical properties, even at ppm levels. Chou et al.[11] investigated the carbon contents of these ceramics with the reaction ^{12}C (d, p) ^{13}C. Carbon profiles for ceramic samples before and after surface cleaning are shown in Figure 6, and indicate significant reduction in the C content following the cleaning process.

Li Profiles in Leached Alloys

Schulte and collaborators[12] used the reaction ^{7}Li (^{3}He, p) ^{9}Be to measure the loss of Li from Al–Li alloys subjected to different environmental treatments. Figure 7 shows some of their results. Because they were interested in measuring how much

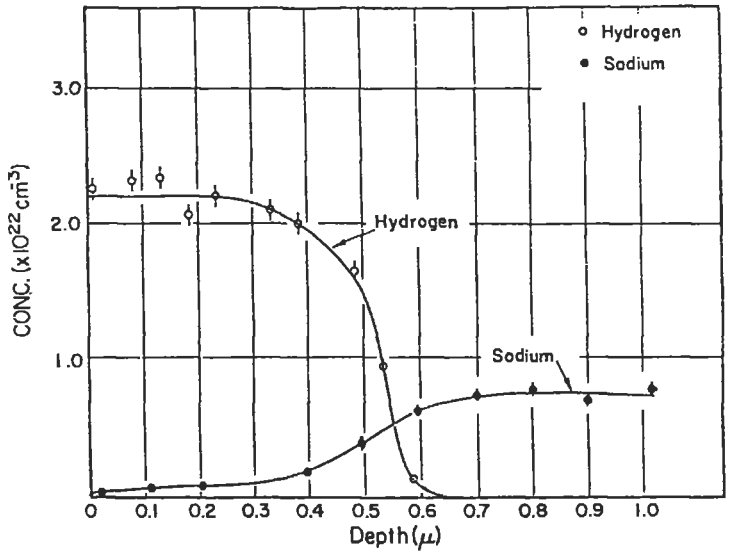

Figure 5 **Hydrogen and sodium profiles of a sample of soda-lime glass exposed to water at 90° C. The Na and H profiles were measured using ^{23}Na (p, γ) ^{24}Mg and ^{1}H (^{15}N, $\alpha\gamma$) ^{12}C resonant nuclear reactions, respectively.[10]**

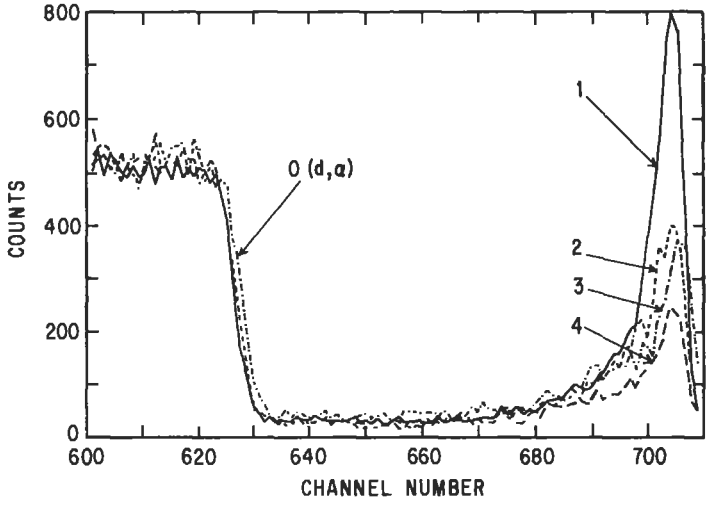

Figure 6 **Spectra of ceramic samples showing effects of surface cleaning on carbon content: (1) spectrum of specimen before cleaning; (2) spectrum of the same specimen after cleaning; (3) and (4) are spectra of two other surface-cleaned specimens.[11]**

Li was leached from a sample as a function of depth into the sample, they mounted the sample in epoxy and measured the Li as a function of distance from the alloy's surface using a finely collimated ^{3}He beam. To know when they were measuring in

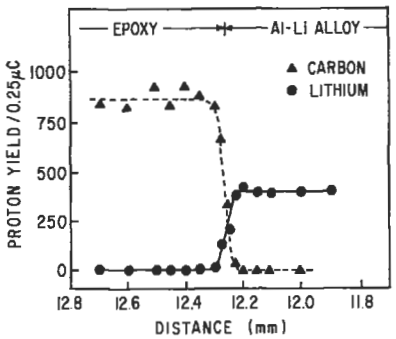

Figure 7 **Lateral profiles of carbon and lithium measured by nuclear reaction analysis. The sample was a lithium alloy mounted in epoxy. As the ion beam was scanned across the epoxy–metal interface, the C signal dropped and the Li signal increased.[12]**

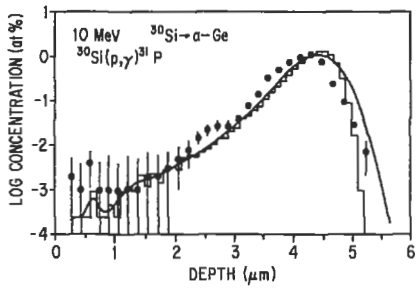

Figure 8 **Profiles of ^{30}Si implanted at 10 MeV into Ge measured by the ^{30}Si (p, γ) ^{31}P resonant nuclear reaction.[13]**

the metal and when in the epoxy, they also monitored the ^{12}C (^{3}He, p) ^{14}N reaction as a measure of the carbon content.

Si Profiles in Germanium

Kalbitzer and his colleagues[13] used the ^{30}Si (p, γ) resonant nuclear reaction to profile the range distribution of 10-MeV ^{30}Si implanted into Ge. Figure 8 shows their experimental results (data points), along with theoretical predictions (curves) of what is expected.

Conclusions

NRA is an effective technique for measuring depth profiles of light elements in solids. Its sensitivity and isotope-selective character make it ideal for isotopic tracer experiments. NRA is also capable of profiling hydrogen, which can be characterized by only a few other analytical techniques. Future prospects include further application of the technique in a wider range of fields, three-dimensional mapping with microbeams, and development of an easily accessible and comprehensive compilation of reaction cross sections.

Related Articles in the Encyclopedia

RBS and ERS

References

1 W. K. Chu, J. W. Mayer, and M. -A. Nicolet. *Backscattering Spectrometry.* Academic Press, New York, 1978, brief section on nuclear reaction analysis, discussions on energy loss of ions in materials, energy resolution, surface barrier detectors, and accelerators also applicable to NRA;

G. Amsel, J. P. Nadai, E. D'Artemare, D. David, E. Girard, and J. Moulin. *Nucl. Instr. Meth.* **92,** 481, 1971, classic paper on NRA, includes discussion of general principles, details on instrumentation, and applications to various fields; G.Amsel and W. A. Lanford. *Ann. Rev. Nucl. Part. Sci.* **34,** 435, 1984, comprehensive discussion of NRA and its characteristics, includes sections on the origin of the technique and applications; F. Xiong, F. Rauch, C. Shi, Z. Zhou, R. P. Livi, and T. A. Tombrello. *Nucl. Instr. Meth.* **B27,** 432, 1987, comparison of nuclear resonant reaction methods used for hydrogen depth profiling, includes tables comparing depth resolution, profiling ranges, and sensitivities.

2 E. Everling, L. A. Koenig, J. H. E. Mattauch, and A. H. Wapstra. *1960 Nuclear Data Tables.* National Academy of Sciences, Washington, 1961, Part I. Comprehensive listing of Q values for reactions involving atoms with $A < 66$.

3 J. W. Mayer, E. Rimini. *Ion Beam Handbook for Material Analysis.* Academic Press, New York, 1977. Useful compilation of information which includes Q values and cross sections of many nuclear reactions for low-Z nuclei. Also has selected γ yield spectra and γ-ray energies for (p, γ) reactions involving low to medium-Z nuclei.

4 J. F. Ziegler. *The Stopping and Range of Ions in Matter.* Pergamon Press, New York, 1980.

5 L. C. Feldman, J. W. Mayer, and S. T. Picraux. *Materials Analysis by Ion Channeling.* Academic Press, New York, 1982.

6 I. Vickridge and G. Amsel. *Nucl. Instr. Meth.* **B45,** 6, 1990. Presentation of the PC program SPACES, used in fitting spectra from narrow resonance profiling. A companion article includes further applications.

7 G. Vizkelethy. *Nucl. Instr. Meth.* **B45,** 1, 1990. Description of the program SENRAS, used in fitting NRA spectra; includes examples of data fitting.

8 Proceedings from Ion Beam Analysis Conferences, in *Nucl. Instr. Meth.* **B45,** 1990; **B35,** 1988; **B15,** 1986; **218,** 1983; **191,** 1981; **168,** 1980.

9 Proceedings from International Conferences on the Application of Accelerators in Research and Industry, in *Nucl. Instr. Meth.* **B40/41,** 1989; **B24/25,** 1987; **B10/11,** 1985.

10 W. A. Lanford, K. Davis, P. LaMarche, T. Laursen, R. Groleau, and R. H. Doremus. *J. Non-Cryst. Solids.* **33,** 249, 1979.

11 N. J. Chou, T. H. Zabel, J. Kim, and J. J. Ritsko. *Nucl. Instr. Meth.* **B45,** 86, 1990.

12 R. L. Shulte, J. M. Papazian, and P. N. Adler. *Nucl. Instr. Meth.* **B15,** 550, 1986.

13 P. Oberschachtsiek, V. Schule, R. Gunzler, M. Weiser, and S. Kalbitzer. *Nucl. Instr. Meth.* **B45,** 20, 1990.

14 G. Amsel and D. Samuel. *Anal. Chem.* **39,** 1689, 1967.